Rock alteration at the post-Variscan nonconformity: implications for Carboniferous-Permian surface weathering versus burial diagenesis and paleoclimate evaluation

Fei Liang[1], Jun Niu[1,2*], Adrian Linsel[1], Matthias Hinderer[1], Dirk Scheuvens[1], Rainer Petschick[3]

[1]Material and Geosciences, Institute of Applied Geosciences, Technical University of Darmstadt, Darmstadt, 64287, Germany
[2]Faculty of Petroleum,China University of Petroleum-Beijing,Karamay Campus, Karamay, 834000, China;
[3]Faculty of Geosciences/ Geography, Goethe-University, Frankfurt, 60438, Germany

Correspondence to: Jun Niu (niujunmm@outlook.com)

Abstract: A nonconformity refers to a hiatal surface located between metamorphic or igneous rocks and overlying sedimentary or volcanic rocks. Those surfaces are key features to understand the relations among climate, lithosphere and tectonic movements during ancient time. In this study, the petrological, mineralogical, and geochemical characteristics of Variscan basement rock and its overlying Permian volcano-sedimentary succession from a drill core in the Sprendlinger Horst, Germany are analyzed by means of polarization microscopy, and environmental scanning electron microscope, X-Ray diffraction, X-ray fluorescence and Inductively Coupled Plasma Mass Spectrometry analyses. In the gabbroic diorite of the basement, the intensity of micro- and macro-fractures increases towards the top indicating an intense physical weathering. The overlying Permian volcanic rock is a basaltic andesite which shows less intense physical weathering compared to the gabbroic diorite. In both segments, secondary minerals are dominated by illite and a mix-layer phase of illite and smectite (I/S). The corrected chemical index of alteration (CIA) and the plagioclase index of alteration (PIA) indicate an intermediate to unweathered degree in the gabbroic diorite and an extreme to unweathered degree in the basaltic andesite. The τ value for both basaltic andesite and gabbroic diorite indicate an abnormal enrichment of K, Rb, and Cs that cannot be observed in the overlying Permian sedimentary rocks. Accompanying minerals such as adularia suggest subsequent overprint by (K-rich) fluids during burial diagenesis which promoted the conversion from smectite to illite. The overall order of element depletion in both basaltic andesite and gabbroic diorite during the weathering process is as follows: Large Ion Lithophile Elements (LILE) > Rear earth elements (REE) > High Field Strength Element (HFSE). Concerning the REE, heavy rare earth elements (HREE) are less depleted than light rare earth elements (LREE). Our study shows that features of supergene physical and chemical paleo-weathering are well conserved at the post-Variscan nonconformity despite hypogene alteration. Both can be distinguished by characteristic minerals and geochemical indices, with the results, a new workflow to eliminate distractions for paleoclimate evaluation and evolution is well developed.

Key words: Weathering; Supergene and hypogene alteration; Elements transfer; Paleoclimate; Permo-Carboniferous; Post-Variscan nonconformity

1 Introduction

Nonconformities refer to contact surfaces between different lithologies in the geological record that were produced over long-lasting periods of non-deposition and/or erosion, which are of paramount importance for the subdivision and correlation of stratigraphic successions (Catuneanu, 1996). They also largely control the geometry of reservoirs for oil, gas, and water (Gardner, 1940). Moreover, nonconformities play a key role in understanding changes of past interactions of atmosphere, hydrosphere, and lithosphere as well as in elucidating driving mechanism for adaption and evolution of life on earth (Fedo et al., 1995; Nesbitt and Young, 1989; Panahi et al., 2000) According to Catuneanu (1996), stratigraphic sequences and bounding surfaces are assigned to different orders based on their relative importance, being also known as a sequence hierarchy.

Especially for continental nonconformities the buried paleo-weathered surfaces provide an ideal opportunity to analyze the weathering and climate conditions during exposure (Jian et al., 2019; Zhou et al., 2017). This includes alteration and deformation of minerals, e.g. changes of crystal morphology of primary and secondary minerals during the weathering process also called supergene alteration (Borrelli et al., 2014). After the paleo-weathered surface was covered by sediments or volcanic rocks, burial commenced leading to increasing temperature and pressure as well as passage of diagenetic fluids. This second overprint during deep burial diagenesis is called hypergene alteration and has to be carefully distinguished from the primary supergene alteration (Dill, 2010).

The widespread post-Variscan nonconformity represents an important first-order bounding surface within the Central and Western European strata. The nonconformity is a result of the denudation of the Variscan orogen which mainly took place from the late Carboniferous to the early Permian (Henk, 1995; McCann, 1999; McCann et al., 2006; Zeh and Brätz, 2004). Locally, however, the contact surface has been overlain at Triassic times at first. So far, the tectonic evolution in Central Europe during post-Variscan times is well studied (Matte, 1991; Ziegler et al., 2004). However, the studies about weathering during the Permo-Carboniferous are fairly scarce. On the other hand, climate and palaeoenvironmental conditions are well known from coal-bearing paralic and lacustrine sediments in the subvariscan foredeep and post-Variscan intramontane basins which indicate an overall aridification trend from humid conditions in the Westphalian to hyperarid conditions in the Guadalupian (Upper Rotliegend). From Lopingian, the climate turned back to semiarid conditions (Roscher and Schneider, 2006).

For the reconstruction of the weathering conditions and the paleoclimate, fine-grained sediments such as siltstone or mudstone are usually investigated (Nesbitt and Young, 1982; Singer, 1988). However, caution is needed as these sediments may be multi-sourced, recycled and/or overprinted during transport and sedimentation (Fedo et al., 1995; Jian et al., 2019). To avoid this, it is feasible to analyze the weathering profile of igneous or metamorphic rocks in the source area itself. With this approach, more accurate in-situ information of the weathering conditions during a certain period can be acquired. This approach also applies to the diagenetic history of the rocks which are situated in direct proximity to the post-Variscan nonconformity (Dill, 2010). The Sprendlinger Horst (Hesse, Germany) is a key area in southwestern Germany for investigating the rock alteration processes at the post-Variscan nonconformity because plutonic Variscan basement rocks are widely covered by only a thin

layer of Cisuralian volcano-sedimentary rocks and the contact surface has been penetrated by numerous drillings (Kirsch et
65 al., 1988).

For this study, we selected a representative drill core reaching from unweathered basement rock into the volcanic-sedimentary
cover which was analyzed at high resolution in particular near the nonconformity. This drill core allowed not only to study
alteration in Variscan basement rocks, but also subsequent alteration of overlying early Permian basalt. We carried out a
detailed petrographical, mineralogical, and geochemical study and applied a new workflow to distinguish the supergene and
70 hypogene alteration processes within a first-order nonconformity. The workflow is based on normalizing mineral types and
geochemical weathering indices to un-overprinted conditions and to quantify the observed deviations. With corrected
geochemical and mineral information of the weathered profile, the weathering and palaeo-climatic condition and the alteration
scenario were addressed.
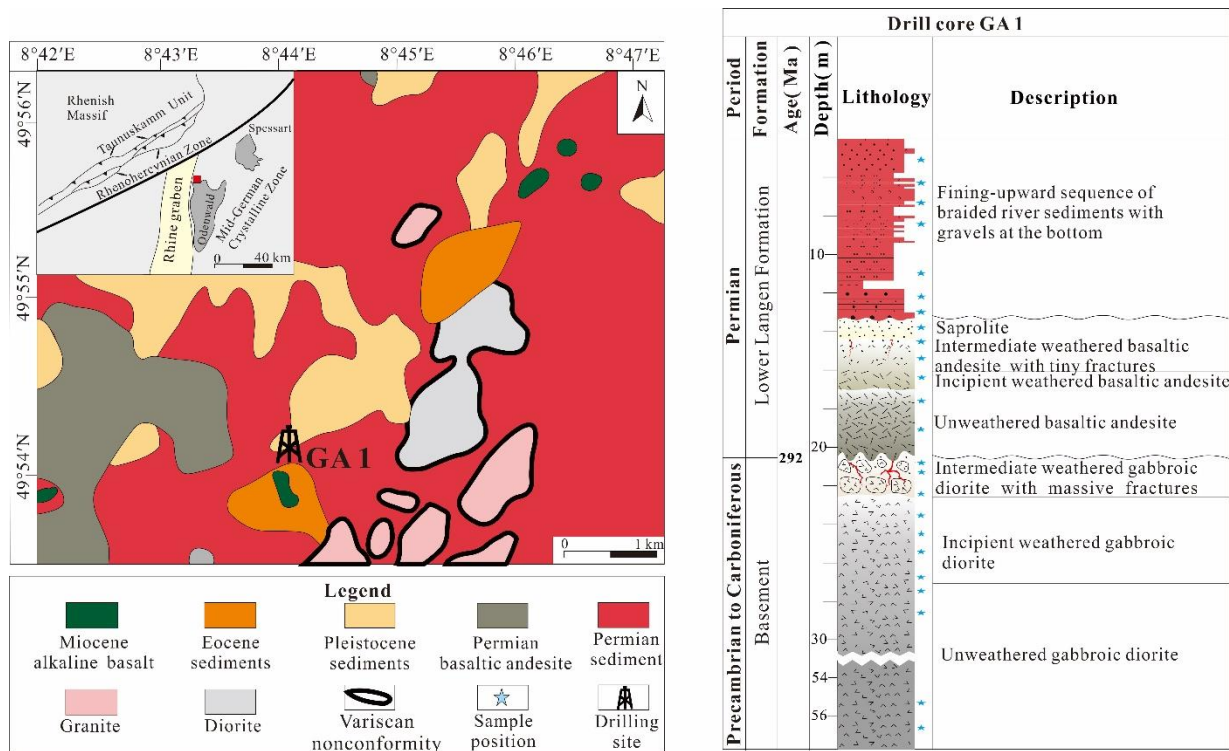
Fig.1. Location and geology of the research area with the lithological section of the drilling GA1; note gap between 30 and 54
m drilling depth. Blue stars indicate sampling spots.

2 Geological Setting

75 The Variscan orogen in Central Europe was formed due to the collision of the mega-continents Gondwana, Laurussia and
intervening microplates, namely Avalonia and Armorica. The final assemblage of these continents led to the formation of

Pangea between ca. 360 and 320 Ma during Carboniferous time (Powell and Conaghan, 1973; Schulmann et al., 2014). Due to a southward-directed subduction of the oceanic lithosphere below the microplate Armorica, the so-called Mid-German Crystalline Zone (MGCZ) was formed as a magmatic arc at the northern margin of Armorica during Early Carboniferous which as a highland continuously weathered and eroded until thermal subsidence began to dominate in Central Europe (von Seckendorff et al., 2004a; Willner et al., 1991; Zeh and Brätz, 2004; Zeh and Gerdes, 2010). As a consequence, the post-Variscan nonconformity was formed, which represents a diachronous time gap of multiple tens to hundred millions years in Central Europe (Henk, 1995; Kroner et al., 2007; von Seckendorff et al., 2004b; Zeh and Brätz, 2004). The weathering surface was covered and hence preserved by Permian sedimentary or volcanic rocks summarized as Rotliegend Group (Becker et al., 2012; Korsch and Schzfer, 1991; Stollhofen, 1998).

The Odenwald basement is the largest basement window of the MGCZ and consists of two major parts which are separated by the Otzberg shear zone: The Bergsträsser Odenwald in the west and the Böllstein Odenwald in the east (Zeh and Gerdes, 2010). The Bergsträsser Odenwald is subdivided into three tectonic units which are composed of magmatic and metamorphic rocks. These are, ordered from north to south, Unit I, which includes the gabbro-dioritic Frankenstein Complex, Unit II with the so-called Neunkirchen Magmatic Suite and Unit III which is dominated by large intrusive bodies of the Weschnitz, Heidelberg and Tromm plutons (Dörr and Stein, 2019; Zeh and Will, 2008). The basement rocks of the so-called Cenozoic Sprendlinger Horst belong to Unit I and represent a northern extension of the Odenwald basement consisting of amphibolite, granite, diorite, gabbroic diorite and gabbro. Geochronological investigations of crystalline rocks of Unit I yield an emplacement age of 362 +/- 9 Ma for the Frankenstein gabbro (Kirsch et al., 1988). K/Ar and ^{40}Ar/^{39}Ar amphibole cooling ages fall into a range between 363 and 334 Ma (Kirsch et al., 1988; Schubert et al., 2001). Cooling below 350 to 300°C (approximate closure temperature for the K-Ar system in biotite) occurred at about 330 Ma (Kirsch et al., 1988). Thermal modeling for the southern Bergsträsser Odenwald implies that the exhumation rate reached a maximum of 1.3 mm/a with average rates of 0.2 mm/a from 338 Ma to 333 Ma (Henk, 1995). Recently, the basement rocks of Unit I of the Sprendlinger Horst were assigned to a Cadomian basement (Dörr and Stein, 2019). The Dieburg metagranite in this region was dated to 540 +/- 8 Ma. According to these new findings the investigated basement rocks are Cadomian relicts in the Variscan orogen.

The Cenozoic Sprendlinger Horst constituted a structural barrier between the nearby Saar-Nahe Basin in the west and the Hessian basin in the east already since the early Cisuralian (McCann, 1999). In the nearby Saar-Nahe Basin a subsidence rate of approximately 0.26 mm/a has been revealed by backstripping analyses for the time between Namurian und Saxonian (Schäfer, 2011). The oldest sedimentary rocks of the Sprendlinger Horst are represented by the Moret Formation (Becker et al., 2012). The Permian Moret Formation deposited in an alluvial environment mostly in wadi-like systems which contain poorly sorted conglomerates, pelites, coarse-grained sandstones/wackes and breccias. The fluvial sedimentary rocks of the overlying Lower Langen Formation are interbedded with basalts and basaltic andesites. These volcanic rocks are the product of a Permo-Carboniferous volcanism which took place throughout Central Europe. Ar^{40}/Ar^{39} dating of the volcanic products in the eastern Saar-Nahe Basin imply ages of around 290 ± 6 Ma (Lippolt and Hess, 1983). This age approximately corresponds to the age of the Donnersberg Formation (Schäfer, 2011). The volcanic products in the Sprendlinger Horst are correlated to

this formation accordingly (Marell, 1989). Mudstone compaction rates indicate that over 3000 m of sediments were eroded due to the inversion of the basin structure during the mid and later Permian (Henk, 1993).

During Permo-Carboniferous time, due to continental climate conditions within the supercontinent Pangea, the paleoclimate in Central Europe graduated from humid to hyperarid conditions (Parrish, 1993). In the Permian and Triassic, only the margins
115 of the supercontinent attracted monsoonal rainfall and showed semiarid to sub-humid condition (Parrish, 1993, 1995). The overall aridization is superimposed by several wet phases, which namely are the Westphalian C/D, the Stephanian A (303.6 Ma to 301.7 Ma), Stephanian C to early Lower Rotliegend (299.1 Ma to 295.5 Ma) and the Early Upper Rotliegend I wet phase (291 Ma to 287 Ma), respectively. These "wet phases" can be observed in the whole European region and are supposed to be linked to deglaciation events of the Gondwana ice cap (Roscher and Schneider, 2006).

120 During the Mesozoic, the tectonic activity in Central Europe was relatively low and accompanied by continuous subsidence and marine transgression. In this phase, around 1500 m of sediments accumulated, which overlaid the Variscan basement and/or Permo-Carboniferous sediments and volcanic rocks (Timar-Geng et al., 2006). Maximum thickness of overburden is expected for the Jurassic (Schäfer, 2011). This is also the period of maximum heating and hydrothermal activity, which overprinted both the Variscan crystalline basement and the overlain sediments and vocanics locally. For this period, also the
125 formation of hydrothermal ores in central and southwest Germany is well documented (Bons et al., 2014; Staude et al., 2011; Timar-Geng et al., 2004). Based on apatite fission track analysis in crystalline rocks of the Odenwald basement, Wagner (1990) estimated temperatures of more than 130°C for in the Jurassic. Burisch et al. (2017) calculated homogenization temperatures from fluid inclusions in hydrothermal veins of 272 to 286°C and 180°C during the middle Jurassic and the Cretaceous, respectively. These temperatures can only be explained by higher heat flow and/or ascending hydrothermal fluids.

130 During the late Cretaceous and the Eocene, coupled to compressional intraplate stress of the Alpine Orogeny, the Upper Rhine Graben system was formed (Behrmann et al., 2005). In conjunction with the formation of the Upper Rhine Graben the Sprendlinger Horst was formed. The latter is bounded by the Rhine Graben fault system in the west and by the Gersprenz graben in the east. Most of the sediments which overlaid the post-Variscan crystalline basement in the research area were eroded since the Cretaceous (Mezger et al., 2013; Schwarz and Henk, 2005). In the nearby southeastern Odenwald region they
135 are partly conserved and reach a thickness of 500 m for the Lower Triassic Buntsandstein (Marell, 1989). On the Sprendlinger Horst only Permian volcano-sedimentary rocks remained which decrease in thickness from north to south of Darmstadt from 250 to 0 m (Marell, 1989; Mezger et al., 2013)

3 Materials and Methods

Numerous drill cores in the Sprendlinger Horst were acquired by a scientific drilling project between 1996 and 2001. Many of
140 the drill cores expose the post-Variscan nonconformity in shallow depths of up to 80 m below ground surface and thus provide a unique chance to investigate this palaeosurface at local scales. Along these drill cores, drilling GA1 was selected because it exposes three different lithological units namely the plutonic basement at the bottom, Permian volcanic lava in the middle and

overlying Permian Rotliegend sedimentary rocks at the top. The sedimentary rocks show a gradual transition from alluvial facies at the base to fluvial facies at the top (Fig. 1) and mainly consist of matrix-rich breccias, wackes and siltstones. Both the

145 top of the basement rock and the top of the volcanic lava constitute palaeosurfaces which faced intense alteration throughout their exposure which is supposed to be significantly shorter for the volcanic rocks. The macroscopic alteration underneath these surfaces is intense which is expressed by a higher degree of fracturing, bleaching and grain disaggregation. The degree of macroscopic alteration decreases with increasing depth in these parts. The core offers the unique opportunity to study subsequent weathering intervals and to compare typical endmembers of rock types with weak (gabbroic diorite) and strong

150 (andesitic basalt) vulnerability to chemical weathering.

In total 24 samples were extracted from the GA1 drill core from which 11 samples belong to the basement, 6 samples to the overlying volcanic rock (Fig. 1) and 7 samples to the sedimentary rocks of the Lower Langen Formation. In order to capture the small-scale petrographic and geochemical variations in the weathering zones appropriately, we reduced the sampling interval in the topmost part of the volcanic rock and in the basement to 40 cm, and for the rest part, to avoid the fractures, the

155 interval is around 1 m.

The samples were used to prepare thin sections which were analyzed by polarization microscopy and SEM/EDX for their petrographic characteristics. For mineral composition, trace element and major element analyses all samples were crushed and milled into a powder with a diameter of less than 63 microns. One part of the powder was examined by X-ray diffraction (XRD) at Goethe University Frankfurt for whole rock mineral composition. The preparations were poor in orientation by careful

160 backside filling of the powder. Using a PANalytical X'Pert diffractometer equipped with a Bragg-Brentano-Goniometer (Copper beam), each sample was scanned under 40 kV and 30 mA for 2 hours. The start angle was 2.5°, the end angle was 70.0° and a step size of 0.008° was applied. The time for each step was 50 s. The mineral phase proportions were estimated by weighted XRD peak intensities after conversion with their typical Reference Intensity Ratios (RIR) as found in the powder diffraction file (PDF-2 and PDF-4 of the International Centre of Diffraction Data: www.icdd.com, see Tab. 1) with the software

165 MacDiff (Petschick et al., 1996).

The powder samples were sent to State Key Laboratory of Isotope Geochemistry, Guangzhou Institute of Geochemistry, Chinese Academy of Science for examination of major elements by X-ray fluorescence (XRF) and examination of trace elements by Inductively Coupled Plasma Mass Spectrometry (ICP-MS). Before XRF analysis, samples were roasted under 900°C for 3 hours and weighed before and after heating to measure the loss on ignition (LOI). Subsequently, 0.51-0.53 g of

170 each sample was mixed with a ratio of 1:8 with $Li_2B_4O_7$ and fused at 1150°C in a Pt-crucible to make a glass disk for XRF analysis.

For trace and rare earth elements analysis, firstly, 40 mg sample powder was weighed and placed into high-pressure-resistant Savillex Teflon beakers to which 0.8 ml 1:1 HNO_3, 0.8 ml HF and 0.5 ml 3N $HClO_4$ was added. The mixture was heated for 48 hours under 100°C and then evaporated. Secondly, 0.8 ml 1:1 HNO_3 was added and heated under 100°C for 12 hours.

175 Thirdly, 0.8ml HF and 0.5ml 3N $HClO_4$ was added and the beaker was sealed and moved into an oven with a temperature of 190°C for 48 hours to make sure the sample was completely dissolved. Fourthly, the beakers were opened, the solution was

evaporated and 4 ml 4N HNO_3 were added. After that, the beakers were sealed and moved into the oven with a temperature of 170°C for 4 hours. Lastly, the solution was diluted with 3% HNO_3 until the weight of the solution was 250 times the weight of the sample. 0.25 g of the solution was taken and diluted with 3% HNO_3 to 2.00 g, mixed with 2.00 g Rh-Re internal standard solution and examined by ICP-MS. To monitor the analytical quality, international standards of GSR-1(granite), GSR-2(andesite), GSR-3(basaltic andesite) were applied.

4 Results

4.1 Petrographic characteristics

4.1.1 Plutonic rock

The Variscan basement in drilling GA1 consists of a coarse-grained plutonic rock with a conspicuous salt-and-pepper appearance and a phaneritic texture. Fractures are pervasive from 20.6 m to 21.4 m and 21.7 m to 22.3 m. The width of the fractures is around 1 cm. From 22.3 m to 23.4 m, both fracture density and width are gradually reducing downwards. Nearly all fractures are filled by secondary minerals (Fig. S1). Under the microscope, the fresh parts of the plutonic basement rock mainly consist of plagioclase (oligoclase and labradorite), quartz, biotite, and amphibole (Fig. 2A). With decreasing depth, primary minerals such as plagioclase and biotite were gradually altered and transformed into secondary minerals, fractures are also ubiquitous in the thin sections in the topmost part. Primary grain shapes are distorted and most of them are filled with calcite (Fig. 2B). And also, recrystallized quartz coupled with calcite is found filled in the fractures (Fig. 2C). Some of the fractures are filled by dolomite accompanied with quartz (Fig. 2D). Even in the topmost part (20.6 m), the plagioclase grains are only partly altered (Fig. 2E).

4.1.2 Lava

The lava has a phaneritic, amygdaloidal texture. Fractures in this part are very limited and occur between 13.8 and 14.7 m with high angle to horizon. The width is less than 1 mm and the fractures are also filled with secondary minerals (Fig. S1). The fresh part of the volcanic rock mainly consists of plagioclase (albite) crystals and amygdaloid bodies which consist of calcite and zeolite locally accompanied with chalcedony (Fig. 2F). With a decrease in depth, the content of plagioclase gradually decreases under the microscope. However, the thin section in the topmost part of the lava (13.9 m) conduct a sudden change, compared with the samples from lower parts. Here nearly all primary minerals were altered to secondary clay minerals but the primary grain shapes are still relatively intact (Fig. 2G). Some residual grains consist of a kaolinite rim and a core of illite or illite-smectite (I-S) mixed layers (Fig. 2H). In the void, adularia with kaolinite can be observed (Fig. 2I).
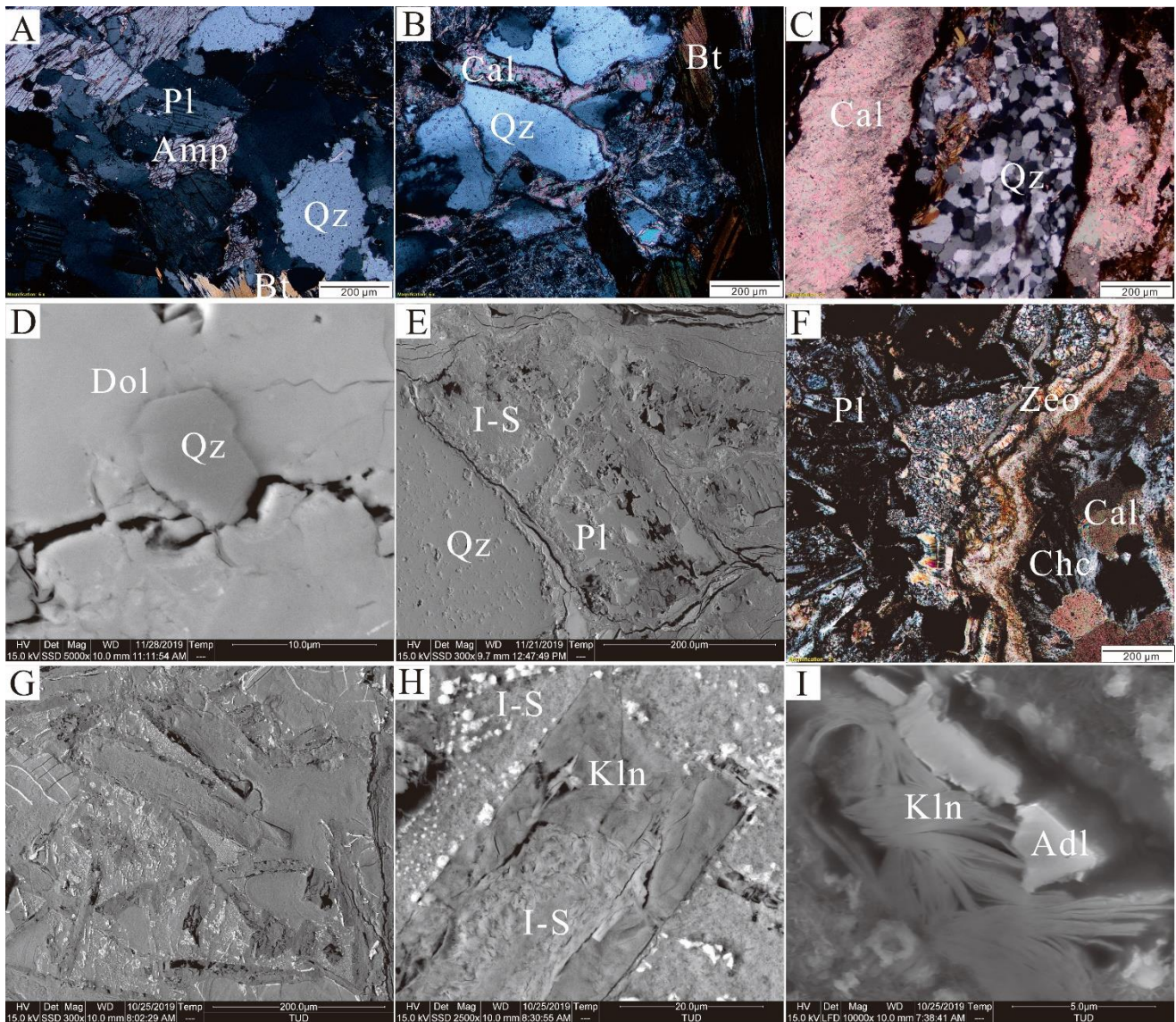
Fig. 2. Petrographic characteristic of the basement and the overlying volcanic rock in the GA1 drill core. (A) fresh gabbroic diorite (PM, z = 55.5 m); (B) gabbroic diorite (PM, z = 20.6 m), fractured quartz grain; (C) gabbroic diorite (PM, z=23.5m), recrystallized quartz coupled with calcite filled in fracture; (D) gabbroic diorite (BSE, z = 21.5 m), dolomite accompanied by quartz; (E) gabbroic diorite (BSE, z = 20.6 m), partly weathered plagioclase. (F) basaltic andesite (PM, z = 17.8 m), fresh plagioclase grains with the amygdaloid consists of calcite and zeolite and chalcedony; (G) basaltic andesite (BSE, z = 13.9 m) secondary clay minerals with intact primary grain shapes; (H) basaltic andesite (BSE, z = 13.9 m), I/S surrounded by kaolinite within one residual plagioclase grain shape; (I) basaltic

andesite (SEM, z = 13.9 m), kaolinite and adularia filled in void; Abbreviations: PM- polarizing microscopy; z-depth below ground surface; Amp-amphibole; Kln-kaolinite; Adl-adularia; Bt-biotite; Cal-calcite; Pl-plagioclase; Zeo-zeolite; Chc-chalcedony; Dol-dolomite; Qz-quartz.

4.2 Mineral Composition

4.2.1 Plutonic rock

The XRD results are listed in the supplementary material (Table S1) and plotted in Fig. 3. The plutonic basement part is composed of plagioclase (oligoclase and labradorite), K-feldspar (only in one sample), quartz, amphibole (mainly Mg-hornblende), and mica phases, with secondary minerals of illite (not separable from micas), vermiculite, I-S mixed layers, minor kaolinite, anatase, hematite, calcite and dolomite. Amphibole abundance decreases in the middle part and disappears in the uppermost part. In the topmost part (20.6-23.5 m) amphibole is not found. Also, plagioclase decreases in abundance from around 40% at the bottom to about 8% at the top. Considering the mineralogical composition of the fresher parts of the plutonic rock, based on the QAPF diagram for plutonic rocks, the protolith of the basement rock can be classified as a quartz diorite/tonalite (Fig. S2), which corresponds well with Mezger (2013).

4.2.2 Lava

The fresh samples of the volcanic rock are composed of augitic pyroxene and plagioclase (albite). In the weathered part, most of the phases appear as secondary minerals, such as quartz, hematite and anatase, and clay minerals such as illite, mixed layer illite-smectite (I-S), vermiculite, and kaolinite, as well as carbonate minerals like calcite and minor dolomite. The uppermost part of the lava is dominated by I/S mixed-layer minerals while the plagioclase content is less than 5% and pyroxene is absent. The abundance of plagioclase (and pyroxene) gradually decreases from bottom to top, and illite and vermiculite exhibit an increasing tendency (fig. 3). Based on the QAPF diagram for volcanic rocks, the protolith of the weathered volcanic rock can be classified as a basalt or andesite (Fig. S2).

4.3 Geochemical characteristics

4.3.1 Geochemical rock classification

In order to further verify the lithological type of the plutonic and volcanic rock in the GA1 drill core, for the basement part, the geochemical data from comparatively fresh samples (23.5-56.5 m) are plotted in the TAS-diagram (Middlemost, 1994) (Fig. 4). Here, the results are mainly plotting in the gabbroic diorite field (Fig. 4A), which is grossly consistent with the results from the petrographic classification (Fig. S2). For the volcanic rock classification, the Revised Winchester-Floyd diagram is applied which is based on immobile trace elements (Pearce, 1996). Most lava samples fall into the andesite/basaltic andesite

field (Fig. 4B), which is in accordance with the petrographic classification result as well. In the following, we use the result of
230 chemical classification and term the two protolith rocks as gabbroic diorite and basaltic andesite.
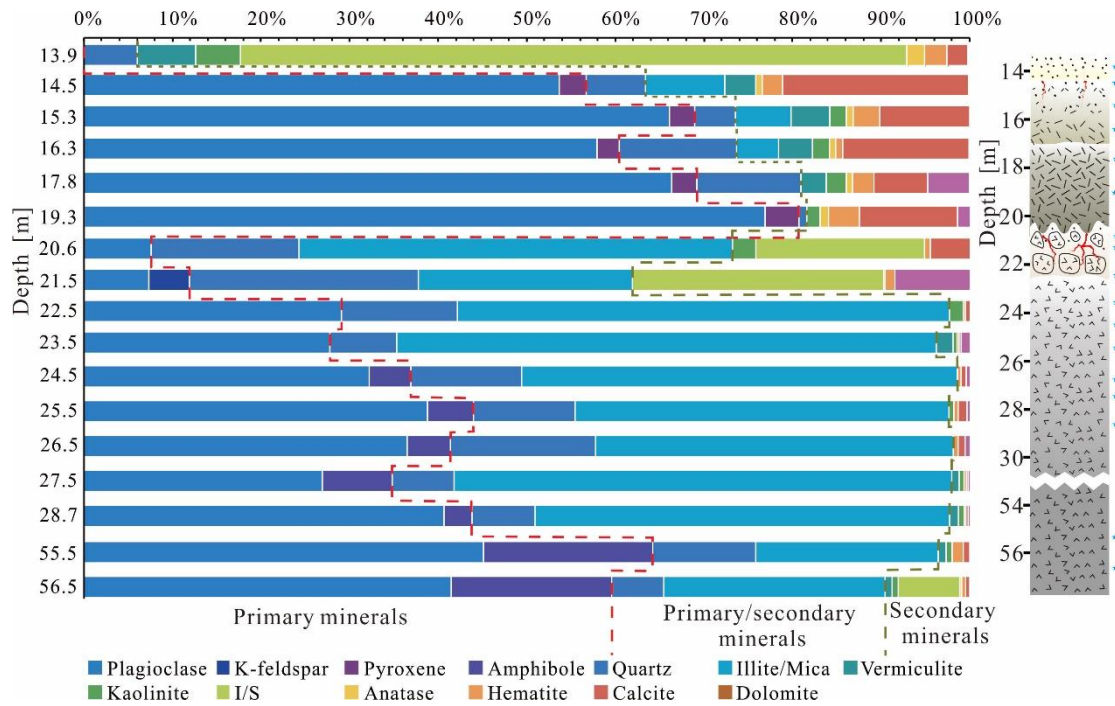
Fig.3. Mineral compositions of both Permian volcanic lava and Paleozoic basement rock in the GA1 drill core

(measured by powder XRD).
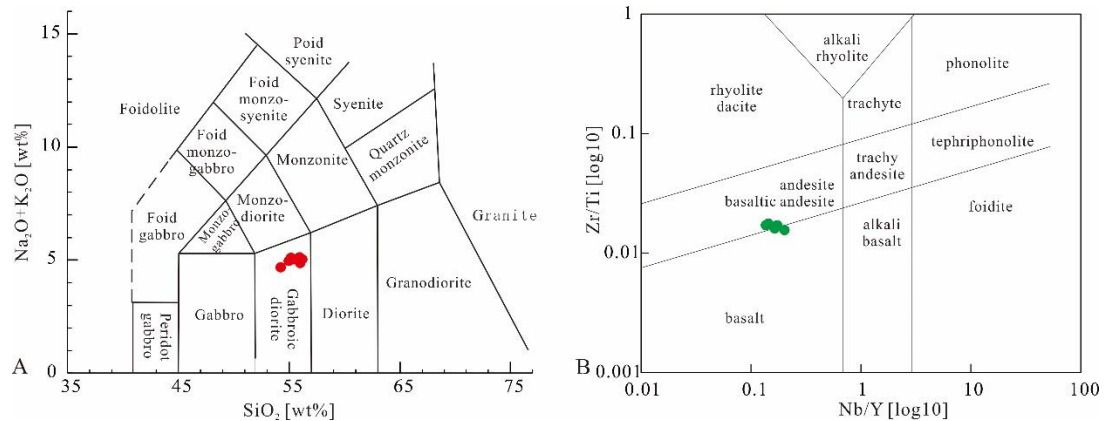
Fig. 4. Classification of rocks of GA1 well with the TAS diagram and Revised Winchester-Floyd diagram. (A)

samples from fresh and nearly fresh parts of basement; (B) samples from overlain lava.

4.3.2 Major elements

The concentrations of major elements are listed in supplementary material (Table S2) and visualized in 1-D profiles for both basaltic andesite (Fig. 5A) and gabbroic diorite (Fig. 5B). Within the lower relatively fresh part of the gabbroic diorite, major
235 elements such as K_2O, Na_2O, P_2O_5 CaO and MnO are almost constant. Al_2O_3 and TiO_2 fluctuate in the topmost part (20.6-21.5 m), and show an overall slightly increasing tendency from top to bottom. For Fe_2O_3, the fluctuation is high in the topmost part and low in the lower part. There is a sharp shift of most concentrations when approaching the intensely altered part at the top of the profile. Despite the high fluctuation of most concentrations in the uppermost part, a significant increase of K_2O and decrease of Na_2O are observed from bottom to top (Fig. 5B).
240 Concerning the basaltic andesite, there are some clear trends with increasing Al_2O_3, K_2O, P_2O_5, and TiO_2 concentrations, and decreasing CaO and Na_2O concentrations towards the top. In contrast to the gabbroic diorite, a sharp shift of concentrations is observed in the uppermost sample for all elements except for Fe_2O_3 which fluctuates along the profile (Fig. 5A).
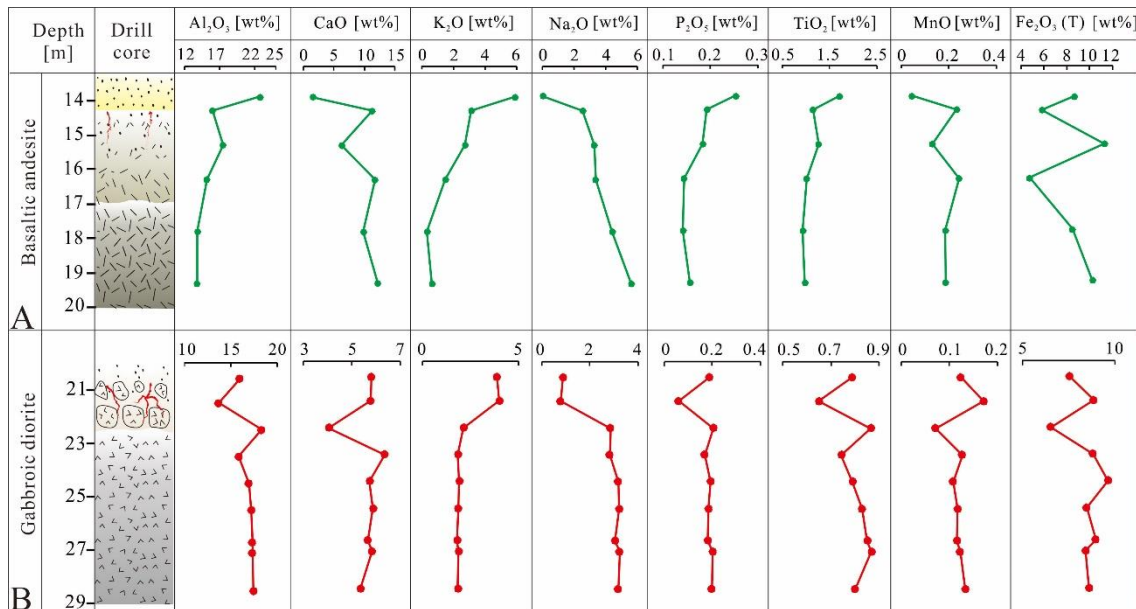
Fig. 5. Major elements content (in wt%) of the basaltic andesite (A) and the gabbroic diorite (B) along the drill core profile.

4.3.3 Trace elements

245 Trace element data is also given in the supplementary material (Table S3). Variations of representative trace elements from both gabbroic diorite and basaltic andesite are shown in Fig. 6. In the gabbroic diorite, except for the topmost part, fluctuations for high field strength element (HFSE) such as Zr, Hf, Nb, Ta and Th (in ppm) are limited or even constant. For large ion

lithophile elements (LILE), Rb and Cs decrease from top to the bottom, whereas Sr increases from 61 ppm to 348 ppm. Ba fluctuates in the upper part of the gabbroic diorite part, but is almost constant in the lower part.

250   Concerning the basaltic andesite part, HFSE such as Zr, Hf, Nb, Ta and Th (in ppm) all exhibit an increasing tendency from bottom to the top with a sharp increase at the topmost sample. LILE such as Rb and Cs also show an increasing tendency, whereas Sr reveals an opposite trend with a decrease from 123 ppm at the bottom to 47 ppm in the topmost part. The tendency for Ba is irregular compared to the other elements, but the overall trend is decreasing.
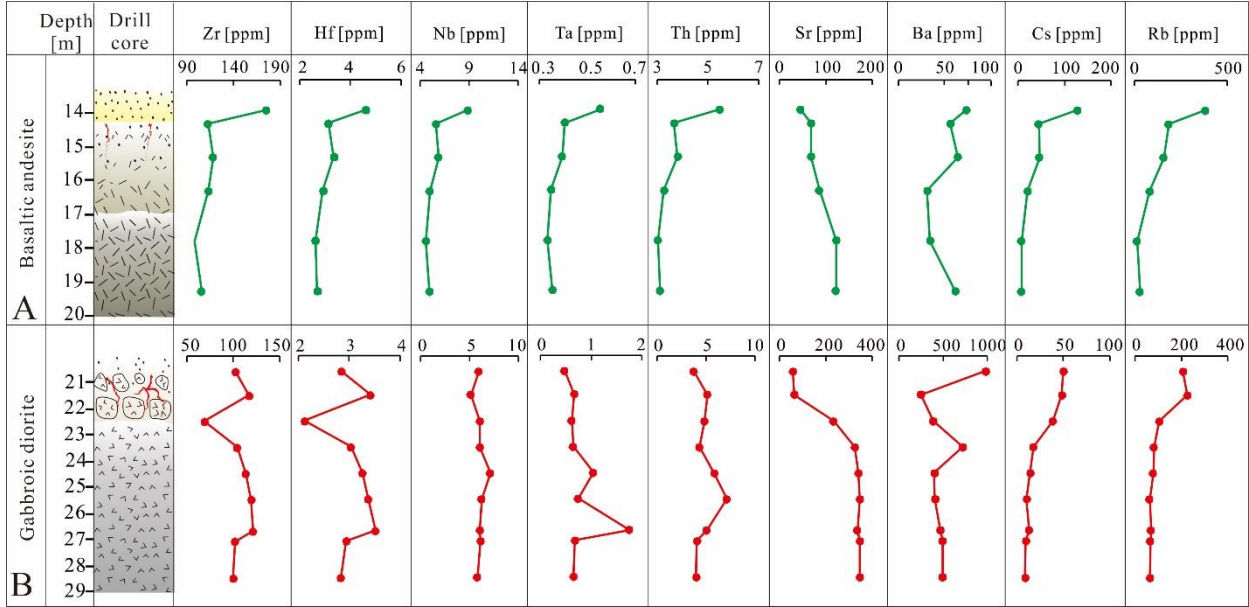
Fig. 6. Representative trace elements content (in ppm) of basaltic andesite (A) and gabbroic diorite (B) along the drill core profile.

4.3.4 Rare Earth Elements (REEs)

255   REE concentrations are listed in supplementary material (Table S4) and are shown as chondrite-normalized patterns (McDonough and Sun, 1995) in Fig. 7. The calculation for the anomalies of cerium (Ce) and europium (Eu) are defined as follows:

$$\frac{Ce}{Ce^*} = \frac{2 \times Ce_N}{La_N + Pr_N},$$ (1)

and

260     $$\frac{Eu}{Eu^*} = \frac{2 \times Eu_N}{(Sm_N + Gd_N)},$$ (2)

The Ce* and Eu* are the hypothetical concentrations of trivalent Ce and Eu, X_N represents the normalized value of the element X. The distribution patterns of both gabbroic diorite and basaltic andesite are nearly parallel in different depths and exhibit

decreasing values from bottom to the top (Fig. 7). All samples are moderately enriched in light rare earth elements (LREEs) and have gently right-dipping REE patterns. They exhibit no Ce anomalies and slightly negative Eu anomalies.
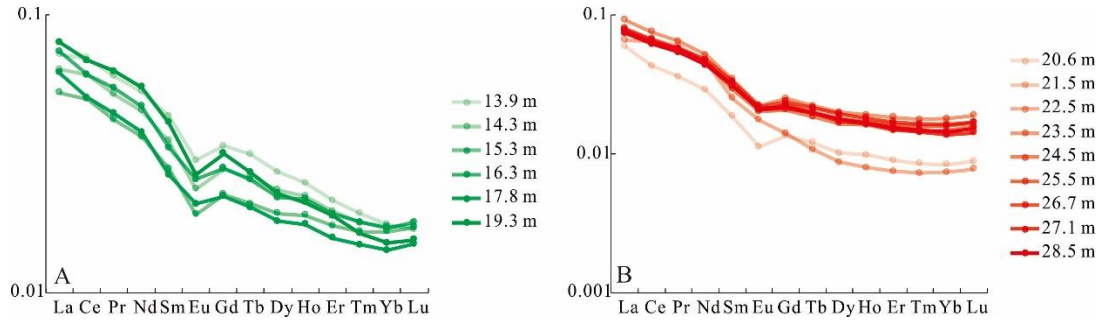
Fig. 7. REE pattern of basaltic andesite (A) and gabbroic diorite (B) in different depths.

5 Discussion

5.1 Chemical alteration

During chemical weathering alkalis and alkaline earth elements contained in silicates such as feldspar, mica minerals, pyroxene and amphibole will be gradually depleted while aluminum tends to remain in situ generating clay minerals (Clift et al., 2014; Nesbitt and Young, 1982; Vázquez et al., 2016). Based on this mechanism, different types of weathering indices were developed to evaluate the weathering intensity. Among those, the Chemical Index of Alteration (CIA) and Plagioclase Index of Alteration (PIA) were proposed by Nesbitt and Young (1982) and Fedo et al (1995), respectively. They are defined as:

$$CIA = \frac{Al_2O_3}{Al_2O_3 + CaO^* + Na_2O + K_2O} \times 100, \tag{3}$$

and

$$PIA = \frac{Al_2O_3 - K_2O}{Al_2O_3 + CaO^* + Na_2O - K_2O} \times 100, \tag{4}$$

All portions are given in molecular weight and in both equations CaO* is the Ca content within silicate minerals only. Bulk rock analysis of altered rocks, however, are affected by Ca mobilisation and secondary calcite precipitation. First, during weathering in the top part Ca may be transferred downward and precipitate there along fractures which were formed before by physical weathering and/or rock relaxation. Second, during burial process Ca may be transferred by fluids from underlying or overlying formations, depending on hydraulic conditions. Both cases will increase the Ca content. Hence, bulk geochemistry cannot be applied directly. For the correction of calcitic CaO*, McLennan (1993) used the following approach : CaO_{rest}= CaO - P_2O_5*10/3, whereas the P_2O_5 is related to apatite, $CaO^* = CaO_{rest}$ when $CaO_{rest}<$ Na_2O, otherwise, $CaO^* = Na_2O$. With this calculation, the CIA value for fresh feldspar is about 50, unaltered basaltic andesite is between 30 and 45, granitoids range between 45 and 55, illite is from 75 to 85, muscovite yields a value of 75 and kaolinite and chlorite have the highest value of

nearly 100 (Fedo et al., 1995). As a modification of the CIA, the PIA value for fresh rock is around 50, and for clay minerals
285 such as kaolinite, illite, and gibbsite it is close to 100 (Fedo et al., 1995; Patino et al., 2003).

In our case, CIA and PIA decrease from top to the bottom for both gabbroic diorite and basaltic andesite. The PIA values are
clearly higher than CIA values (Fig. 8A). In the topmost basaltic andesite part the CIA is up to 77, which indicates an
intermediate degree of weathering. The results from XRD and BSE, however, indicate that the plagioclase is weathered and
74% of the constituent is I/S. This is well expressed by the PIA, which yields a value of 98, hence, the PIA is more consistent
290 with the mineralogical and petrographic character compared to the CIA.
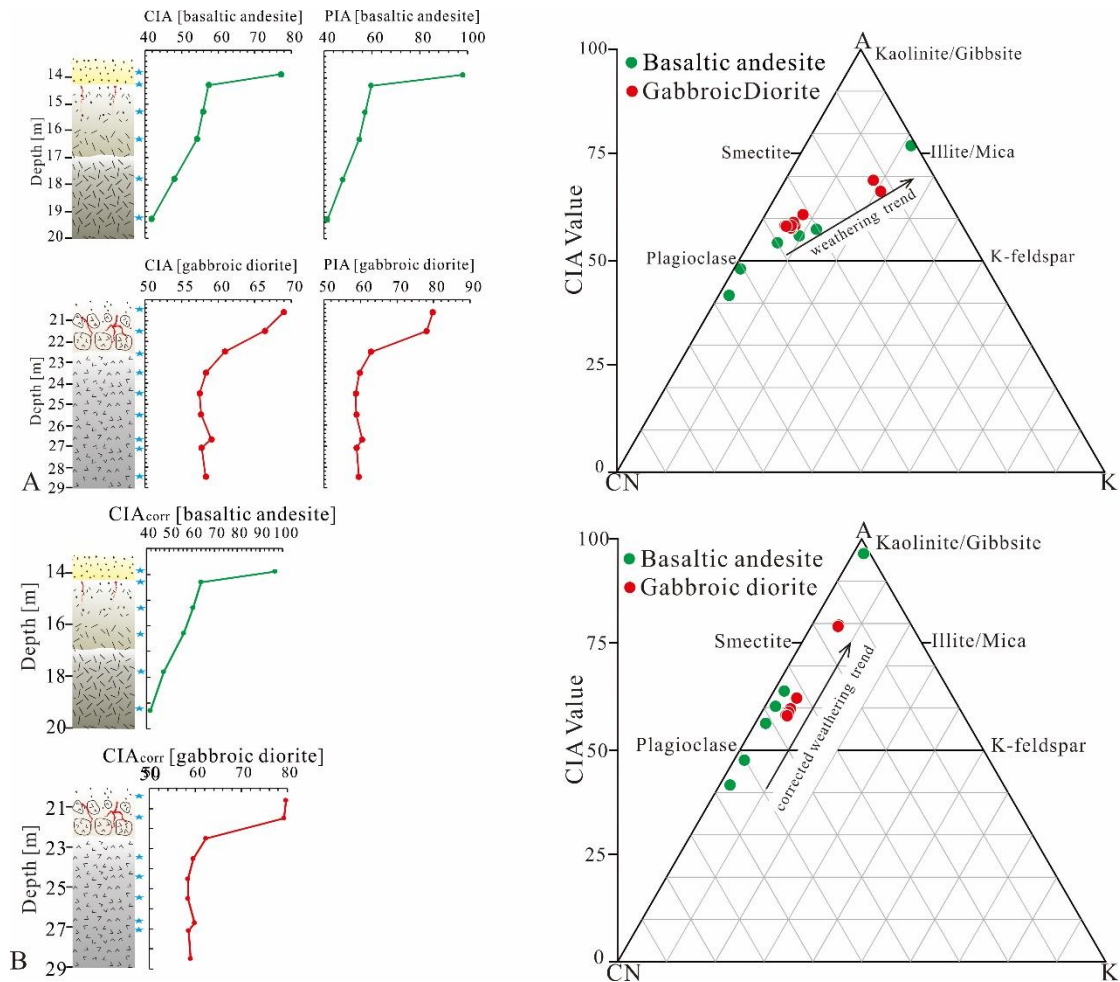
Fig. 8. Weathering indices with A-CN-K diagram of both basaltic andesite and gabbroic diorite before and after K

correction; based on (Fedo et al., 1995; Nesbitt and Markovics, 1997).

To better evaluate the weathering intensity, the A-CN-K ternary diagram is applied (Fedo et al., 1995; Nesbitt and Young,
1984). The letter A stands for Al_2O_3, CN for (CaO^*+Na_2O) and K is the content of K_2O all in molecular proportions. The ideal
weathering trend for different types of parent rocks in the upper continental crust should be parallel to the A-CN axis, but due

to diagenetic alteration the original data tend to deviate from the theoretical weathering trend (Babechuk et al., 2015; Fedo et al., 1995; Zhou et al., 2017). The trends for both basaltic andesite and gabbroic diorite samples uniformly deviate from the ideal weathering tendency and excurse to the K apex (Fig. 8A), which clearly indicates a relative K enrichment. In the literature, the enrichment of K is interpreted as K metasomatism due to conversion among clay minerals such as the transformation from kaolinite to illite, or from plagioclase to K-feldspar (Fedo et al., 1995; Nesbitt and Young, 1984; Zhou et al., 2017). K metasomatism results in a lower CIA value relative to the actual weathering intensity and can also explain the deviation from the PIA. To address this problem, Fedo et al. (1995) suggested that the proportion of "pre-metasomatic" compositions of the weathering products could be determined by correcting each point on the A-CN-K diagram back to its predicted position. The method proposed by Panahi et al. (2000) for the K correction is applied:

$$K_2O_{corr} = \frac{m*A_w + m*CN_w}{1-m} \tag{5}$$

The A_w and CN_w refer to the Al_2O_3 and (CaO^*+Na_2O) content in the weathering zone, where

$$m = \frac{K}{A+CN+K} \tag{6}$$

and the K, A and CN values for the calculation of **m** were taken from the protolith sample.

With corrected K_2O values, the trend of all sample points in the A-CN-K diagram is parallel to the A-CN axis (Fig. 8B). Moreover, the CIA_{corr} values are now consistent with the PIA value. The CIA_{corr} values of the gabbroic diorite indicate an intermediate to incipient chemical weathering degree with CIA_{corr} values of 80 at the top part and 58 at the bottom (Fig. 8B). PIA values decrease from 83 to 59 (Fig. 8B). For both CIA_{corr} and PIA values, inconsistent trends between the topmost (20.6-21.5 m) and the rest part (22.5-28.5 m) result from a sudden decrease of the weathering degree which form a "discontinuity". The CIA_{corr} and PIA values in the topmost part range from 79 to 80 and 78 to 80 respectively, and in the rest part, the CIA_{corr} and PIA values decrease from 62 to 58 and 63 to 59. Petrographic and mineralogical features correspond well with the corrected weathering indexes. Secondary alteration products are mainly illite, with a small quantity of kaolinite and vermiculite.

The corrected CIA values in the basaltic andesite suggest an extreme to incipient weathering degree with CIAcorr and PIA values decreasing from 97 and 98, respectively, at the top to 42 and 41 at the bottom. Similar to the gabbroic diorite, for both CIAcorr and PIA values a discontinuity exists between the topmost part (13.9 m) and the lower part (14.3-19.3 m). The high CIAcorr and PIA values in the topmost part of the basaltic andesite indicate extreme chemical weathering. In the lower part of the basaltic andesite, CIAcorr and PIA values decrease from 64 at the top to 42 at the bottom and from 65 to 41, respectively (Fig. 8B). These values are much lower than values from the topmost part and suggest an incipient weathering degree. Based on the XRD results, the plagioclase content at the bottom is 77% and declines gradually upsection to 54% in 14.5 m before it suddenly drops to 0% in 13.9 m. In 14.5 m depth, the plagioclase grains are still mostly fresh, which is clearly different from the uppermost half meter in which they are completely altered.

5.2 Quantification of elements transfer

For quantification of element transfer due to weathering and diagenesis the τ model is applied (Anderson et al., 2002; Nesbitt, 1979; Nesbitt and Markovics, 1997). The model uses the relation between the mobile element concentration in the sample (M_{sample}) vs. protolith ($M_{protolith}$), and the immobile element concentration in the sample (I_{sample}) vs. protolith ($I_{protolith}$). Among the immobile elements, Ti is widely used as a key element (Middelburg et al., 1988). Thus the model is defined as:

$$\tau_M = \frac{M_{sample} \times Ti_{protolith}}{M_{protolith} \times Ti_{sample}} - 1 , \tag{7}$$

When $\tau_M > 0$, element M is enriched during alteration, when $\tau_M = 0$, element M is immobile during alteration, when $0 > \tau_M > -1$, element M is depleted, when $\tau_M = -1$, element M is completely lost from the material. For the basaltic andesite and gabbroic diorite, the samples from the bottom (19.3 m and 55.5 m, 56.5 m, respectively) were selected as protoliths to provide the lowest degree of alteration based on CIA values, petrographic features and XRD results.

The results for major and trace elements are listed in supplementary material (Table S5) and are plotted in Fig. 9. In the basaltic andesite part, both Ca and Na are strongly depleted in the topmost part (13.9 m) with τ_{Ca} and τ_{Na} of -0.93 and -0.99 respectively. τ_{Ca} gradually increases from -0.60 to -0.07 and τ_{Na} from -0.60 to -0.18 with increasing depth from 14.3 m down to 17.8 m. The discontinuity between the topmost and the rest part correspond well with the CIA and PIA value. However, in the gabbroic diorite part, the τ_{Na} values from the top gradually increase from -0.70 (20.6 m) to -0.67 (21.5 m), followed by a sharp increase in the lower part with values between -0.12 and 0.06. This is consistent with the trends of both CIA and PIA. τ_{Ca} values show a high variability compared to τ_{Na}. The sample from 20.6 m yields a τ value of -0.03 which indicates a slight depletion of Ca while the sample from 21.5 m shows a τ value of 0.17, which suggests a slight enrichment of Ca (Fig. 9B). A similar enrichment also occurs in 23.5 m, which yields a value of 0.13 (Table S5).

The Sr/Ca ratio can be applied as a parameter to distinguish different phases of diagenetic fluids (Berndt et al., 1988; Brandstätter et al., 2018). To figure out the source of Ca, the Sr-CaO diagram is applied (Fig. 9A). The ratio of Sr/CaO at the top of the gabbroic diorite in 20.6 m and 21.5 m depth show a close relation with the Sr/CaO ratios of the basaltic andesite and clearly deviate from the general trend of the gabbroic diorite and the overlying sedimentary rocks. This hints to a chemical overprint of the gabbroic diorite by the overlying basaltic andesite, whereas the Ca in the lower part appears to be primary. The spike of τ_{Ca} in 23.5 m depth can also be explained by porosity data (Weinert et al., 2020) which can be considered being a measure of fracture density and grain disaggregation in igneous rocks. The porosity decreases sharply from 24% in 21.5 m to 3% in 23.6 m depth (Fig. 9B). This can be explained by the fact that before the Permian basaltic to andesitic lava flow flooded the basement, the fractures provided pathways for meteoric water. Ca was leached by meteoric water and transferred downward through these fractures and accumulated around the interface, where the porosity sharply decreases.

Based on K_{corr}, K was depleted during the weathering process, in both basaltic andesite and gabbroic diorite. The depletion trend of K from top to the bottom is similar to the trend of Na. In the topmost part of the basaltic andesite, τ_{Kcorr} is -0.59 and gradually increases to -0.35 and 0.08 from 14.3 m to 17.8 m depth. In the top part of the gabbroic diorite, τ_{Kcorr} increases from

-0.26 (20.6 m) to -0.23 (21.5 m) followed by a sharp increase to around 0 in the lowest part (Table S5). The τ value trend of K$_{corr}$ is in agreement with macroscopic and microcopic weathering trends which supports the applicability of the K correction. In contrast to Ca and Na, elements closely related to clay formation such as K, Rb and Cs show significant enrichment (Fig. 6). In the gabbroic diorite part, the τ values of K, Rb and Cs decrease from 2.5 to 0.2, from 5.4 to 0.5 and from 19.8 to 2.3 from top to bottom, respectively. Similarly, they decrease in the basaltic andesite from 4.2 to -0.4, from 5.5 to -0.4, and from 8.4 to 0.2.
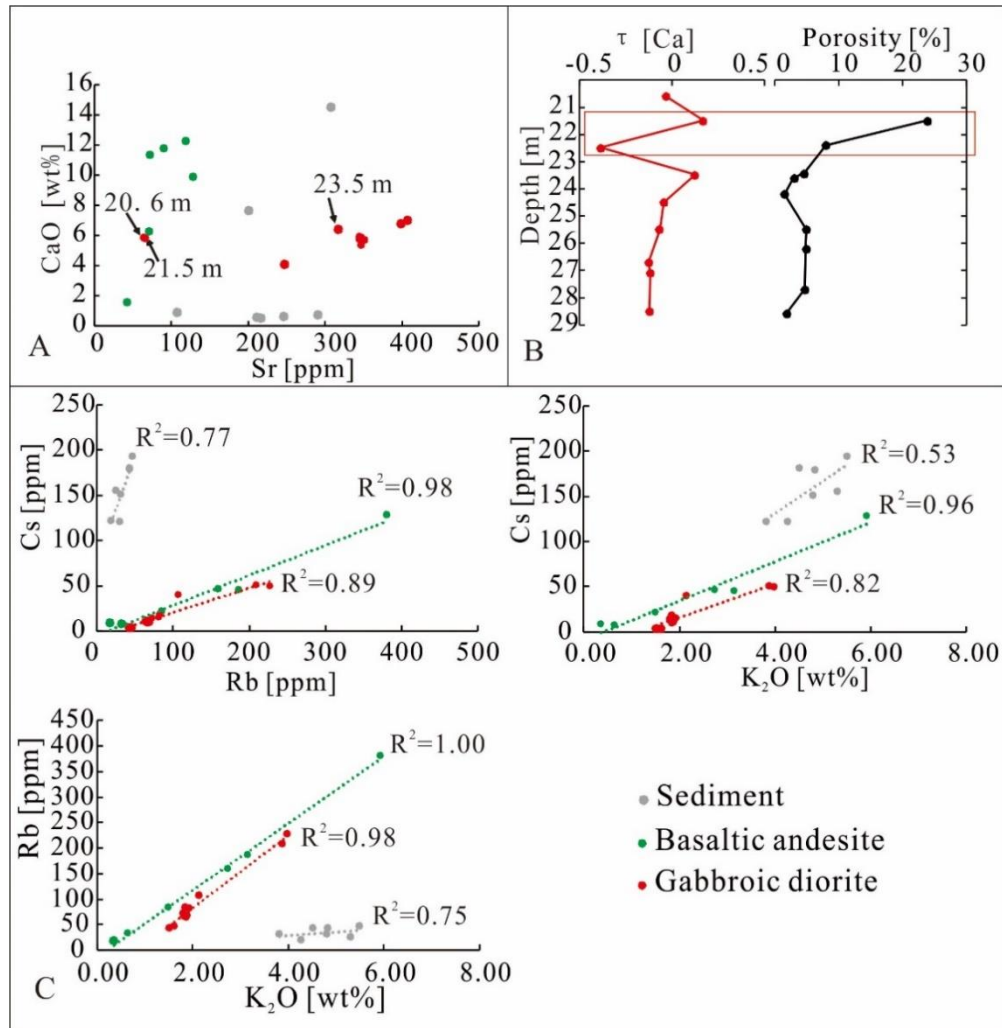
Fig. 9. Elements characteristics, (A) CaO-Sr cross-plot for GA1 drill core; (B) Relationship between the τ value and the porosity in the gabbroic diorite; (C) Relationship among Rb, Cs and K$_2$O for sedimentary rocks, basaltic andesite and gabbroic diorite.

To search for the origin of this enrichment, correlation diagrams for gabbroic diorite, basaltic andesite, and sediments are plotted (Fig. 9C). The linear and close relationships between Cs, Rb and K in the gabbroic diorite and basaltic andesite point to a joint alteration of both, whereas the overlying sediments can be excluded as a source. This is consistent with the conclusion of Molenaar et al.(2015), who claimed that the overlain Permian Rotliegend sediment on Sprendlinger Horst formed a "closed system" and diagenetic fluids did not transfer matter in and out of the system. Palmer and Edmond (1989) claimed that mobile elements such as K, Rb and Cs are very easily being extracted by thermal fluids and transferred during hydrothermal activity. In addition to clay transformation, typical minerals formed from hot fluids are observed in thin-sections and XRD such as dolomite with accompanied secondary quartz and adularia (Fig. 3). This observation supports the model of a second alteration which was pervasive through the nonconformity and must have happened during burial diagenesis.

Fig. 10 displays the τ_M values for all elements. The LILE elements K, Rb and Cs are removed from the figure due to their strong enrichment which would affect the scaling of all other elements. The remaining large ion lithophile elements (LILE) Sr and Ba are enriched in the gabbroic diorite but depleted in the basaltic andesite. Most probably the enrichment in the gabbroic diorite is associated with diffusive carbonate precipitation which is missing in the basaltic andesite.
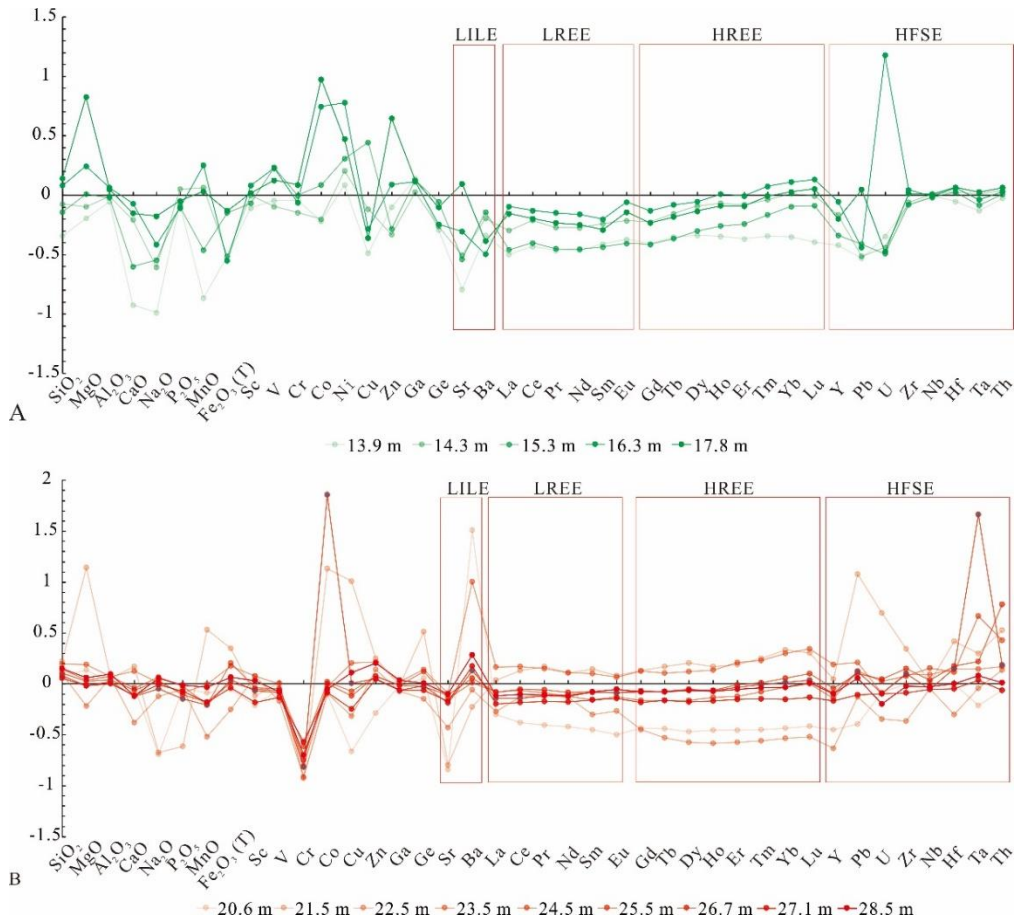
Fig. 10. τ value features of basaltic andesite (A) and gabbroic diorite (B) in GA1 well

In both gabbroic diorite and basaltic andesite, the τ values gradually increase from LREE to HREE (Fig. 10). This indicates that the depletion degree from LREE to HREE is reducing during the alteration process if the same conditions exist. In a study of weathering of a granodiorite, Nesbitt (1979) showed that REE are removed by acidic leaching of meteoric water which

380   becomes buffered with depth and loses its etching effect due to rising pH. Moreover, Nesbitt (1979) proposed that the fractionation of LREE and HREE may be controlled by the mineral type. Kaolinite and illite are favorable for LREE while vermiculite, Fe-Ti-oxy-hydroxides, relict hornblende and biotite are more favorable for HREE. In our study, the reducing depletion degree from LREE to HREE in both weathering profiles also indicate that in the same acid weathering environment LREE are more mobile than HREE. Also, REE fractionation of the gabbroic diorite is less systematic from top down compared

385   with the basaltic andesite (Fig. 10B). By comparison with rock textures, we assume that this is due to physical fracturing and more heterogeneous chemical alteration in the basement. The strongly depleted samples at 20.6 m and 22.5 m depth are close to fracture zones and possibly more affected by leaching. In contrast, the enriched samples from 21.5 m and 23.5 m depth are without macro-fractures. This can be explained by acidic meteoric water which used the pathways provided by the macro-fractures in the topmost part of the gabbroic diorite. REEs in the fracture zone were leached and transported downward and

390   accumulated around the interface of macro-fracture and macro-fracture-free zone. This is comparable to the behaviour of Ca. The high field strength elements (HFSE) Zr, Nb, Hf, Ta and Th are expected to be immobile. In the gabbroic diorite the τ values scatter significantly for specific elements within single samples. The samples in 21.5 m and 23.5 m depth show mostly enriched values together with Pb and U, which is in line with REE. Other element shifts appear to be controlled by heterogeneous conservation and alteration of specific minerals due to the fractured and granular texture of the rock. The

395   depletion of Pb and U can be well explained by oxidation during weathering into the mobile species Pb^{6+} and U^{4+}, respectively and subsequent leaching by meteoric water. In addition, from LILE to HFSE, the overall depletion degree decreased in both basaltic andesite and gabbroic diorite part during alteration process.

5.3 Burial diagenesis and its implications for weathering intensity evaluation

In addition to correct the alteration trend, the A-CN-K diagram can also be used to kinetically predict the primary weathering

400   products of plutonic and volcanic rocks (Nesbitt and Young, 1984; Panahi et al., 2000). In this case, this concept is applied to differentiate surface weathering from burial diagenesis by comparing the remaining secondary minerals in the profile with the theoretical weathering products.
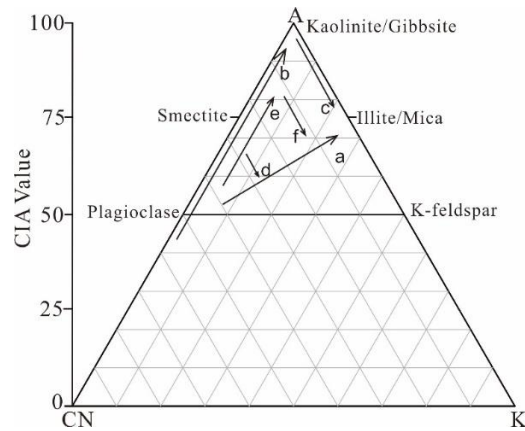
Fig. 11. Theoretical weathering trend during burial diagenesis (Fedo et al., 1995), a = observed weathering trend for both basaltic andesite and gabbroic diorite; b = theoretical weathering trend for basaltic andesite; c = K-metasomatism trend of topmost basaltic andesite; d = K-metasomatism trend of the lower part of basaltic andesite; e = theoretical weathering trend for gabbroic diorite; f = K-metasomatism trend for gabbroic diorite.

Rock types which contain only minor amounts of K tend to be weathered directly by forming smectite and kaolinite instead of
405 illite regardless under what kind of climate owing to the chemical composition restriction (Nesbitt and Young, 1989). In our
case, both gabbroic diorite and basaltic andesite contain minor K. However, secondary minerals mainly consist of illite which
makes metasomatic addition of this element during burial diagenesis highly probable (Fedo et al., 1995). As discussed in
section 5.2, K-metasomatism is possibly promoted by hydrothermal fluids. According to the A-CN-K diagram (Fig. 11), the
initial weathering products of the gabbroic diorite should have mainly consisted of smectite, and in the top part (20.6-21.5 m)
410 a small quantity of kaolinite is expected. For the basaltic andesite (13.9 m) kaolinite with a small portion of smectite is expected,
whereas smectite should be dominant in the lower part. ESEM imaging indicated kaolinite in two morphologies: the vermiform
(Fig. 2H) and booklet form (Fig. 2I). According to Chen et al. (2001) and Erkoyun and Kadir (2011), vermiform kaolinite is
favoured during in situ formation of kaolinite, while the euhedral booklet form is favoured during autogenic diagenesis (e.g.
Bauluz et al. (2008). Kaolinite formed by chemical weathering is always more anhedral (Bauluz et al., 2008; Varajao et al.,
415 2001), therefore, the influence from subrecent surface related weathering can be excluded in our case. Based on the XRD
results of the gabbroic diorite (Fig. 3), the remaining mineral in the topmost part (13.9 m) of the basaltic andesite is I/S, which
can be explained by the conversion of kaolinite and smectite into I/ S. Na and Ca as needed for the I/S formation may originate
from the original smectite or from diagenesis fluids. The τ values of Na and Ca in the topmost part are -0.99 and -0.93,
respectively, therefore, the influence on the CIA and PIA values for evaluating the weathering intensity is negligible. The
420 remaining secondary mineral in the lower part (14.3-19.3 m) is illite, which can be explained by conversion of smectite into
illite. During this process, the Ca and Na within the original smectite should be further depleted, and this will increase the CIA
and PIA values, with the decrease content of secondary mineral, this influence will also decrease, and in this case, due to the
low content of the first secondary minerals formed under lower chemical weathering degree, the depletion of Ca and Na content

should also be limited as well as the CIA and PIA values. Similar to the basaltic andesite, in the gabbroic diorite, the first secondary minerals formed by weathering predominantly was smectite according to the A-CN-K diagram. During the overprint of diagenesis, the smectite was transformed into I/S in the topmost part (20.6- 21.5 m), in the lower part (22.5-28.5 m) the smectite was all transformed into illite. Hence, the Ca and Na should be depleted and CIA and PIA increased. In the topmost part, this influence should be highest and decreases with decreasing content of the secondary minerals towards the lower part. In both basaltic andesite and gabbroic diorite, the illitisation makes K addition from outside the system necessary, most probably by fluid migration through fractures. The smectite resulting from weathering in the gabbroic diorite would have been altered to pure illite in the presence of sufficient K. As we observe a high amount of I/S, K supply was not sufficient to alter the smectite completely to illite in the topmost part of the gabbroic diorite (20.6-21.5 m). A similar mineral content pattern also exists in the basaltic andesite. The illite in the lower part (14.3-16.3 m) was most probably transformed from smectite. However, K supply was not enough in the topmost part where I/S and residual kaolinite are dominant (13.9 m) (Fig. 3).

5.4 Implications for paleoclimate

The occurrence of weathering products, such as illite, smectite and kaolinite can be applied as a useful tool to assess the paleoclimate (Clift et al., 2014; Raucsik and Varga, 2008; Singer, 1988). However, caution should be paid while working with these parameters as clay minerals may be overprinted by transformation or neoformation during burial diagenesis, and the restriction due to the geochemical composition of rock type as it is discussed in section 5.3. It follows that, when the clay minerals in the sedimentary rocks are investigated to assess paleoclimatic conditions, the lithology of the source rocks should be considered. In particular for the weathering profile of the igneous rock, all the involved processes mentioned above will lead to misjudgements of paleoclimate conditions if working with raw data. Taking this study as an example, and interpreting the original data from XRD and SEM analysis, I/S clay minerals would indicate a subhumid climate with prominent dry seasons (Raucsik and Varga, 2008; Singer, 1988). For the deeper parts of both basaltic andesite and gabbroic diorite, the clay minerals are dominated by illite, pointing to a cold or dry climate. According to this information, the profile would suggest that the climate alternated twice from a cold and dry climate to a seasonal and alternating wet and dry climate. However, due to the limited K availability, the dominant illite in gabbroic diorite and basaltic andesite must be a product of a diagenetic overprint. When correcting the A-CN-K diagram, the primary weathering product in the topmost part of the gabbroic diorite must have been smectite with negligible illite and possibly a small quantity of kaolinite (20.6-21.5 m). Furthermore, smectite can also not be applied to evaluate the paleoclimatic conditions in this case due to the K limitation of the lithology.

Although CIA and PIA values may be misleading sometimes, they display well the alteration intensity of the gabbroic diorite with much higher values in the topmost part (20.6-21.5 m). However, a related tendency of the HFSE is not existent (Fig. 6B). Due to leaching, these immobile elements are expected to become indirectly enriched, which is not observed. HFSE values and τ values of representative LILE, such as Na and Sr, show a positive correlation with porosity data, which suggests the intensity of the leaching process was more dominated by the porosity formed by intense physical weathering, rather than by other factors such as climate shifting to more humid conditions.

Correction of the A-CN-K diagram for the basaltic andesite part suggests that primary products of the altered basaltic andesite in the topmost part (13.9 m) were dominated by kaolinite and in the lower part mainly by smectite. Again, smectite cannot be applied as a climate parameter due to the restriction of K content in basaltic andesite. Similar to the gabbroic diorite part, the CIA and PIA values, the mineral abundances and the petrographic features significantly change between the topmost part (13.9 m) and the lower part (14.3-19.3 m). In contrast to the gabbroic diorite, however, the relative content of high field-strength elements (HFSEs) such as Nb, Ta, Zr, Hf and Ti are all drastically shifted between the topmost part (13.9 m) and the lower part (Fig. 6A). The abnormal relative concentrations of these elements in the topmost part indicate more depletion of other relatively more mobile element, which is confirmed by the τ value of Na and Ca. All parameters together, i.e. CIA, PIA, relative content of clay mineral types (additional kaolinite in the topmost part), and petrologic features, indicate that the climate changed to humid conditions during basalt weathering. Moreover, the thin saprolite layer demonstrates that surficial weathering lasted only for a short period and that the basalt was rapidly covered by alluvial sediments.

As mentioned in section 5.2, the weathering environment for the basaltic andesite was more acidic than for the gabbroic diorite. The acid present in the weathered profile can be attributed to CO_2 input from the atmosphere or organic acids produced by vegetation. Based on the drill core profile, vegetation was undeveloped at the paleosurfaces on both gabbroic diorite and basaltic andesite parts, respectively. Hence, the increased acid was probably due to an increase of CO_2 in the atmosphere (Berner, 1992; Neaman et al., 2005), which may also be the reason for the deglaciation event during the Permo-Carboniferous.

6 Scenario for alteration at the post-Variscan nonconformity

As the weathering process and the paleoclimate is elucidated, the overall alteration process at the post-Variscan nonconformity can be separated into three subsequent steps (Figs. 12-14). Approximately at the Carboniferous/Permian boundary, the gabbroic diorite was firstly weathered under relatively arid conditions. This included fracturing by physical weathering and moderate chemical weathering. Plagioclase was transformed to smectite with negligible illite (Fig. 12, Eq. 1&2). Other minerals such as amphibole and biotite were weathered to smectite and chlorite accompanied by the generation of hematite and vermiculite (Fig. 12, Eq. 3-5). With the beginning of volcanism in the early Permian, the nonconformity was concealed by the basaltic andesite lava flow, which underwent a short, but intense period of chemical weathering. Firstly, pyroxene and plagioclase were weathered to vermiculite and smectite (Fig. 13, Eq. 6 & 7). Thereafter, more humid conditions initiated increased leaching and smectite was transformed to kaolinite (Fig. 13, Eq. 8). During these two stages, elements such as Na, Ca and K were depleted from the system, either by export or descendent enrichment in the profile. After a relatively short time interval, the basalt was concealed by sediments and the weathering process terminated. During burial diagenesis, fluids transformed smectite and kaolinite into illite in both gabbroic diorite and basaltic andesite (Fig. 13, Eq. 9&10). The transformation of smectite to illite led to depletion of Ca and Na as well. This leaching process is accompanied by the formation of accessory minerals such as quartz, dolomite, calcite and adularia (Fig. 14, Eq. 11&12), which indicate a temperature around 200°C (Stimac et al., 2015). Emplacement of calcitic veins is partly coupled with low-temperature migration recrystallization

quartz (Fig. 2C), which indicates a temperature of around 300°C (Stipp et al., 2002). This roughly coincides with temperatures

490 from thermochronological apatite fission track studies in the surrounding basement of the Odenwald which indicate heating up to more than 130°C before 80 to 105 Ma and homogenization temperatures from fluid inclusions in hydrothermal veins up to ca. 290°C (Wagner et al., 1990, Burisch et al. 2017). Subsidence ceased in the uppermost Jurassic as evident from surrounding sedimentary sequences in southern Germany. Relative stability can be expected until the early Cenozoic, when the European Cenozoic Rift System was initiated also forming the Sprendlinger Horst (Ziegler et al., 2004). Since the Eocene,

495 the Mesozoic sedimentary cover of the Sprendlinger Horst was subsequently removed. Most probably, exhumation of the basement did not take place before the upper Miocene (Sissingh, 2003). A further pulse of exhumation is proven for the middle to late Pleistocene (Lang, 2007).
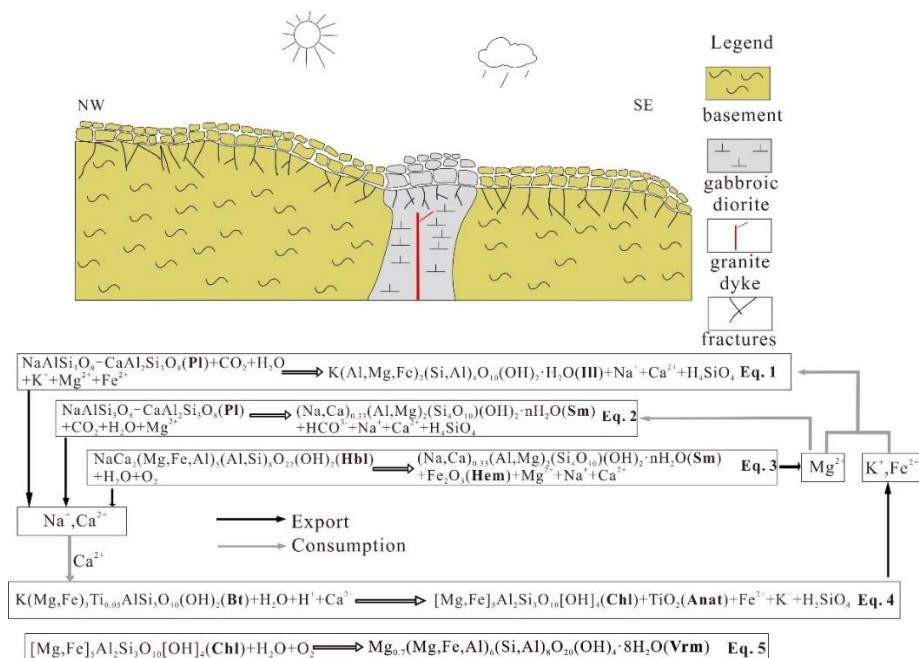
Fig. 12. Reconstructed alteration model of GA1 well in Sprendlinger Horst before volcanic eruption around ca. 300 Ma; Abbreviations: Anat- anatase; Bt-biotite; Chl-chlorite; Hbl-hornblende; Hem-hematite; Ill-illite; Pl-plagioclase; Sm-smectite; Vrm-vermiculite.
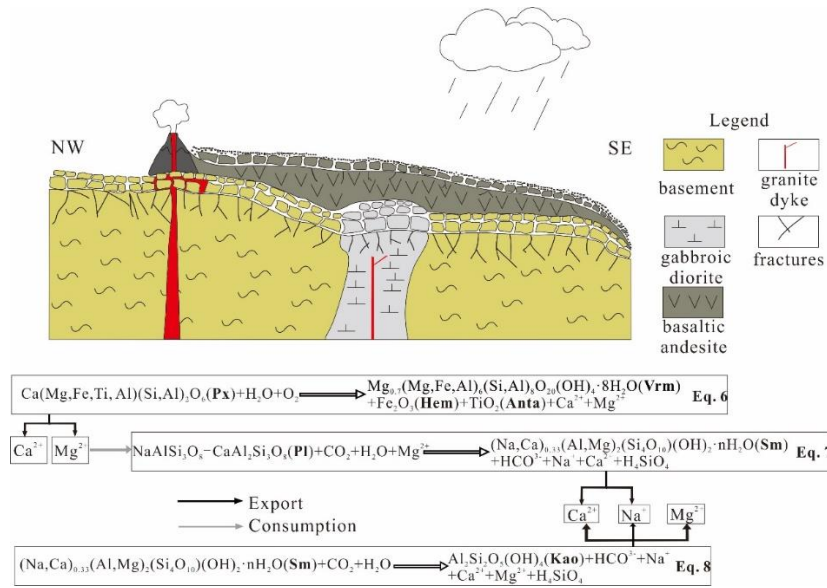
Fig. 13. Reconstructed alteration model of GA1 well in Sprendlinger Horst after volcanic eruption around 290 Ma; Abbreviations: Px-pyroxene.
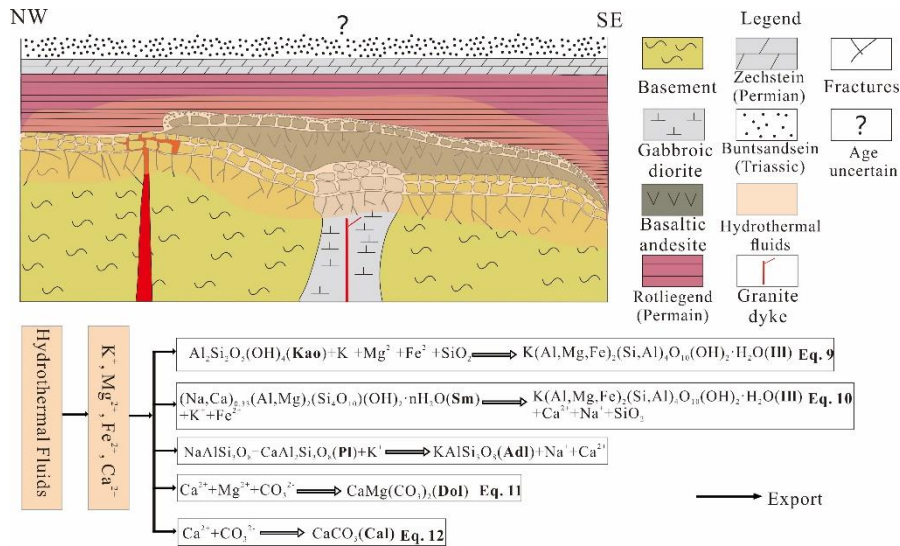
Fig. 14. Reconstructed alteration model of GA1 well in Sprendlinger Horst during burial in the Jurassic and Cretaceous; Abbreviations: Adl- adularia.

7. Conclusions

A combined study of mineralogy, petrography and geochemistry is performed on a drill core, that penetrates the post-Variscan nonconformity on the Sprendlinger Horst (southwestern Germany). The aim of this study was to elucidate rock alteration at and across the nonconformity and to disentangle surficial weathering and its overprint by burial diagenesis. The unconformity

is covered by a Permian lava flow followed by alluvial sediments of the Rotliegend. This allows to study two different lithologies and two subsequent periods of surficial weathering together with burial diagenesis affecting both in a later stage. The crystalline basement is composed of a gabbroic diorite, whereas the lava flow is a basaltic andesite.

505 In the gabbroic diorite, mineralogical and geochemical parameters show a gradual alteration trend with a maximum depth of around 10 m, whereas the andesitic basalt shows shallower and more intense alteration with complete chemical alteration in the topmost part. Chemical alteration goes along with physical alteration which is evident from fracture density. The different alteration steps were separated using thin section analysis, clay mineralogy, and geochemistry. In addition, trends in the A-CN-K diagram and element transfer ratios were used to determine pristine rock compositions.

510 Surficial weathering of both gabbroic diorite and basaltic andesite are all indicated by petrographic characteristics, increasing abundance of secondary minerals, increasing CIA and PIA values, and enrichment of immobile HFSE due to leaching process. In the gabbroic diorite, ubiquitous now filled fractures with width around 1 cm in the upmost part (20.6-21.4 m) suggests intense physical weathering, combined with chemical weathering preferentially along these fractures. Corrected clay mineral composition yield smectite with negligible illite and possibly a small quantity of kaolinite pointing to an arid climate. Physical

515 weathering in the basaltic andesite is much weaker compared to the gabbroic diorite. An overprint by burial diagenesis is indicated by K metasomatism, clay mineral transformation and neoformation of minerals, as well as enrichment of K, Rb and Cs in the alteration zone. In both, gabbroic diorite and andesitic basalt, the primary weathering products such as smectite and kaolinite were transformed into illite, and this will also have some influences on the evolution of weathering intensity.

At both nonconformities, distinct gradients from the top downward demonstrate that surficial weathering is the major alteration

520 process. During burial diagenesis, fluids preferentially percolated along the post-Variscan non-conformity and at the basalt/sediment boundary, due to a higher permeability. This led to clay mineral transformation and some neoformation of minerals, but did not change the alteration pattern. Deeper parts of both parent rocks are pristine and not affected neither by surficial weathering nor by fluids during burial diagenesis.

Our case study shows that surface weathering in the past has a prime control on the petrography and geochemistry, and also

525 guides fluids through the system during burial diagenesis. Moreover, we could demonstrate that formation of the saprolite zone depends on rock composition, climatic conditions, as well as the duration of the process. Our results have implications for paleoclimatic and burial diagenetic studies. In order to separate hypergene and supergene alteration, we provide a workflow for nonconformities and shed light on the use of paleo-weathering surfaces for paleoclimate research.

Sample availability

530 All samples are available at the Institute of Applied Geoscience, TU Darmstadt and can be requested from liang@geo.tu-darmstadt.de.

Author contribution

Liang Fei conceptualized and prepared the paper, Niu Jun provided the foundation and contributed to the conceptualization, Dirk Scheuvens and Rainer Petschick conducted the SEM and XRD measurements, Matthias Hinderer and Adrian Linsel overall supervised this research.

Competing interests

The authors declare that they have no conflict of interest.

Acknowledgement

Geochemical analysis for this work was co-funded by "University research program of Xinjiang province (No. XJEDU2019Y070)", "Innovation talent project of Karamay (No. 2019RC002A)" and China Scholarship Council (CSC). The authors would like to thank Senckenberg Research Station of Grube Messel, Dr. Sonja Wedmann and Mr. Bruno Behr who provided drill cores for this work and Mr. Reimund Rosmann who provided a lot of help. We highly appreciate the constructive reviews of Reinhard Gaupp and Henrik Friis.

Reference

Anderson, S. P., Dietrich, W. E. and Brimhall, G. H.: Weathering profiles, mass-balance analysis, and rates of solute loss: Linkages between weathering and erosion in a small, steep catchment, GSA Bull., 114(9), 1143–1158, doi:10.1130/0016-7606(2002)114<1143:wpmbaa>2.0.co;2, 2002.

Babechuk, M. G., Widdowson, M., Murphy, M. and Kamber, B. S.: A combined Y/Ho, high field strength element (HFSE) and Nd isotope perspective on basalt weathering, Deccan Traps, India, Chem. Geol., 396, 25–41, doi:10.1016/j.chemgeo.2014.12.017, 2015.

Bauluz, B., Mayayo, M. J., Yuste, A. and González López, J. M.: Genesis of kaolinite from Albian sedimentary deposits of the Iberian Range (NE Spain): analysis by XRD, SEM and TEM, Clay Miner., 43(3), 459–475, doi:10.1180/claymin.2008.043.3.10, 2008.

Becker, A., Schwarz, M. and Schäfer, A.: Lithostratigraphische Korrelation des Rotliegend im östlichen Saar-Nahe-Becken Lithostratigraphic Correlation of the Rotliegend in the eastern Saar-Nahe Basin., 2012.

Behrmann, J. H., Ziegler, P. A., Schmid, S. M., Heck, B. and Granet, M.: The EUCOR-URGENT project. Upper Rhine Graben: Evolution and neotectonics, Int. J. Earth Sci., 94(4), 505–506, doi:10.1007/s00531-005-0513-0, 2005.

Berndt, M. E., Seyfried, W. E. and Beck, J. W.: Hydrothermal alteration processes at midocean ridges: experimental and theoretical constraints from Ca and Sr exchange reactions and Sr isotopic ratios, J. Geophys. Res., 93(B5), 4573–4583,

560   doi:10.1029/JB093iB05p04573, 1988.

Berner, R. A.: Weathering, plants, and the long-term carbon cycle, Geochim. Cosmochim. Acta, 56(8), 3225–3231, doi:10.1016/0016-7037(92)90300-8, 1992.

Bons, P. D., Fusswinkel, T., Gomez-Rivas, E., Markl, G., Wagner, T. and Walter, B.: Fluid mixing from below in unconformity-related hydrothermal ore deposits, Geology, 42(12), 1035–1038, doi:10.1130/G35708.1, 2014.

565   Borrelli, L., Perri, F., Critelli, S. and Gullà, G.: Characterization of granitoid and gneissic weathering profiles of the Mucone River basin (Calabria, southern Italy), Catena, 113, 325–340, doi:10.1016/j.catena.2013.08.014, 2014.

Brandstätter, J., Kurz, W., Richoz, S., Cooper, M. J. and Teagle, D. A. H.: The Origin of Carbonate Veins Within the Sedimentary Cover and Igneous Rocks of the Cocos Ridge: Results From IODP Hole U1414A, Geochemistry, Geophys. Geosystems, 19(10), 3721–3738, doi:10.1029/2018GC007729, 2018.

570   Catuneanu: Principles of sequence stratigraphy, 1st Editio., ELSEVIER SCIENCE & TECHNOLOGY, Oxford, United Kingdom., 1996.

Chen, P. Y., Wang, M. K. and Yang, D. S.: Mineralogy of dickite and nacrite from Northern Taiwan, Clays Clay Miner., 49(6), 586–595, doi:10.1346/CCMN.2001.0490608, 2001.

Clift, P. D., Wan, S. and Blusztajn, J.: Reconstructing chemical weathering, physical erosion and monsoon intensity since

575   25Ma in the northern South China Sea: A review of competing proxies, Earth-Science Rev., 130, 86–102, doi:10.1016/j.earscirev.2014.01.002, 2014.

Dill, H. G.: Authigenic heavy minerals a clue to unravel supergene and hypogene alteration of marine and continental sediments of Triassic to Cretaceous age (SE Germany), Sediment. Geol., 228(1–2), 61–76, doi:10.1016/j.sedgeo.2010.04.006, 2010.

580   Dörr, W. and Stein, E.: Precambrian basement in the Rheic suture zone of the Central European Variscides (Odenwald), Int. J. Earth Sci., 108(6), 1937–1957, doi:10.1007/s00531-019-01741-7, 2019.

Erkoyun, H. and Kadir, S.: Mineralogy, micromorphology, geochemistry and genesis of a hydrothermal kaolinite deposit and altered Miocene host volcanites in the Hallaçlar area, Uşak, western Turkey, Clay Miner., 46(3), 421–448, doi:10.1180/claymin.2011.046.3.421, 2011.

585   Fedo, C. M., Wayne Nesbitt, H. and Young, G. M.: Unraveling the effects of potassium metasomatism in sedimentary rocks and paleosols, with implications for paleoweathering conditions and provenance, Geology, 23(10), 921, doi:10.1130/0091-7613(1995)023<0921:uteopm>2.3.co;2, 1995.

Gardner, F. J.: Relationship of unconformities to oil and gas accumulation, , 24, 2022–2031, 1940.

Henk, A.: Subsidenz und Tektonik des Saar-Nahe-Beckens (SW-Deutschland)., 1993.

590   Henk, R. A.: Late Variscan exhumation histories of the southern Rhenohercynian Zone and western Mid-German Crystalline Rise: results from thermal modeling., 1995.

Jian, X., Zhang, W., Liang, H., Guan, P. and Fu, L.: Mineralogy, petrography and geochemistry of an early Eocene weathering profile on basement granodiorite of Qaidam basin, northern Tibet: Tectonic and paleoclimatic implications, Catena, 172, 54–64, doi:10.1016/j.catena.2018.07.029, 2019.

595   Kirsch, H., Kober, B. and Lippolt, H. J.: Age of intrusion and rapid cooling of the Frankenstein gabbro (Odenwald, SW-Germany) evidenced by40Ar/39Ar and single-zircon207Pb/206Pb measurements, Geol. Rundschau, 77(3), 693–711, doi:10.1007/BF01830178, 1988.

Korsch, R. J. and Schzfer, A.: Geological interpretation of DEKORP deep seismic reflection profiles 1C and 9N across the Variscan Saar-Nahe Basin, southwest Germany., 1991.

600   Kroner, U., Hahn, T., Romer, R. L. and Linnemann, U.: The variscan orogeny in the saxo-thuringian zone - Heterogenous overprint of Cadomian/Paleozoic Peri-Gondwana crust, in Special Paper of the Geological Society of America, vol. 423, pp. 153–172, Geological Society of America., 2007.

Lang and Stefan: Die geologische Entwicklung der Hanau-Seligenstädter Senke (Hessen, Bayern)., 2007.

Lippolt, H. J. and Hess, J. C.: Isotopic evidence for the stratigraphic position of the Saar-Nahe Rotliegend volcanism I.

605   40Ar/40K and 40Ar/39Ar investigations, Neues Jahrb. für Geol. und Paläontologie - Monatshefte, 1983(12), 713–730, doi:10.1127/njgpm/1983/1983/713, 1983.

Marell, D.: Das Rotliegende zwischen Odenwald und Taunus, , 128 p. [online] Available from: file://catalog.hathitrust.org/Record/102424593, 1989.

Matte, P.: Accretionary history and crustal evolution of the Variscan belt in Western Europe, Tectonophysics, 196(3–4),

610   309–337, doi:10.1016/0040-1951(91)90328-P, 1991.

McCann, T.: The tectonosedimentary evolution of the northern margin of the Carboniferous foreland basin of NE Germany, Tectonophysics, 313(1–2), 119–144, doi:10.1016/S0040-1951(99)00193-6, 1999.

McCann, T., Pascal, C., Timmerman, M. J., Krzywiec, P., López-Gómez, J., Wetzel, A., Krawczyk, C. M., Rieke, H. and Lamarche, J.: Post-Variscan (end Carboniferous-Early Permian) basin evolution in Western and Central Europe, Geol. Soc.

615   Mem., 32, 355–388, doi:10.1144/GSL.MEM.2006.032.01.22, 2006.

McDonough, W. F. and Sun, S. s.: The composition of the Earth, Chem. Geol., 120(3–4), 223–253, doi:10.1016/0009-2541(94)00140-4, 1995.

McLennan, S. M.: Weathering and Global Denudation'. [online] Available from: http://www.journals.uchicago.edu/t-and-c, 1993.

620   Mezger, J. E., Felder, M. and Harms, F. J.: Kristallingesteine in den maarablagerungen von Messel: Schlüssel zum verständnis der geometrien der messel-störungszone und des vulkanschlots und der posteruptiven beckenentwicklung, Zeitschrift der Dtsch. Gesellschaft fur Geowissenschaften, 164(4), 639–662, doi:10.1127/1860-1804/2013/0034, 2013.

Middelburg, J. J., Van Der Weijden, C. H. and Woittiez, J. R. W.: Chemical processes affecting the mobility of major, minor and trace elements during weathering of granitic rocks, 1988.

625   Middlemost, E. A. K.: Naming materials in the magma/igneous rock system., 1994.

Molenaar, N., Felder, M., Bär, K. and Götz, A. E.: What classic greywacke (litharenite) can reveal about feldspar diagenesis: An example from Permian Rotliegend sandstone in Hessen, Germany, Sediment. Geol., 326, 79–93, doi:10.1016/j.sedgeo.2015.07.002, 2015.

Neaman, A., Chorover, J. and Brantley, S. L.: Implications of the evolution of organic acid moieties for basalt weathering over geological time, Am. J. Sci., 305(2), 147–185, doi:10.2475/ajs.305.2.147, 2005.

Nesbitt, H. W.: Mobility and fractionation of rare earth elements during weathering of a granodiorite., 1979.

Nesbitt, H. W. and Markovics, G.: Weathering of granodioritic crust, long-term storage of elements in weathering profiles, and petrogenesis of siliciclastic sediments., 1997.

Nesbitt, H. W. and Young, G. M.: Early proterozoic climates and plate motions inferred from major element chemistry of lutites, Nature, 299(5885), 715–717, doi:10.1038/299715a0, 1982.

Nesbitt, H. W. and Young, G. M.: Prediction of some weathering trends of plutonic and volcanic rocks based on thermodynamic and kinetic considerations, Geochim. Cosmochim. Acta, 48(7), 1523–1534, doi:10.1016/0016-7037(84)90408-3, 1984.

Nesbitt, H. W. and Young, G. M.: Formation and diagenesis of weathering profiles. J. Geol.,[online] Available from: http://www.journals.uchicago.edu/t-and-c, 1989.

Palmer, M. R. and Edmond, J. M.: Cesium and rubidium in submarine hydrothermal fluids: evidence for recycling of alkali elements., 1989.

Panahi, A., Young, G. M. and Rainbird, R. H.: Behavior of major and trace elements (including REE) during Paleoproterozoic pedogenesis and diagenetic alteration of an Archean granite near Ville Marie, Québec, Canada., 2000.

Parrish, J. T.: Climate of the supercontinent Pangea, J. Geol., 101(2), 215–233, doi:10.1086/648217, 1993.

Parrish, J. T.: Geologic Evidence of Permian Climate, in The Permian of Northern Pangea: Volume 1: Paleogeography, Paleoclimates, Stratigraphy, edited by P. A. Scholle, T. M. Peryt, and D. S. Ulmer-Scholle, pp. 53–61, Springer Berlin Heidelberg, Berlin, Heidelberg., 1995.

Patino, L. C., Velbel, M. A., Price, J. R. and Wade, J. A.: Trace element mobility during spheroidal weathering of basalts and andesites in Hawaii and Guatemala, Chem. Geol., 202(3–4), 343–364, doi:10.1016/j.chemgeo.2003.01.002, 2003.

Pearce, J. A.: A User's Guide to Basalto Discriminant Diagrams, Geol. Assoc. Canada, Short Course Notes, 79–113, 1996.

Petschick, R., Kuhn, G. and Gingele, F.: Clay mineral distribution in surface sediments of the South Atlantic: Sources, transport, and relation to oceanography, Mar. Geol., 130(3–4), 203–229, doi:10.1016/0025-3227(95)00148-4, 1996.

Powell, C. M. A. and Conaghan, P. J.: Plate tectonics and the Himalayas, Earth Planet. Sci. Lett., 20(1), 1–12, doi:10.1016/0012-821X(73)90134-9, 1973.

Raucsik, B. and Varga, A.: Climato-environmental controls on clay mineralogy of the Hettangian-Bajocian successions of the Mecsek Mountains, Hungary: An evidence for extreme continental weathering during the early Toarcian oceanic anoxic event, Palaeogeogr. Palaeoclimatol. Palaeoecol., 265(1–2), 1–13, doi:10.1016/j.palaeo.2008.02.004, 2008.

Roscher, M. and Schneider, J. W.: Permo-Carboniferous climate: Early Pennsylvanian to Late Permian climate development

660   of central Europe in a regional and global context, Geol. Soc. Spec. Publ., 265, 95–136,

doi:10.1144/GSL.SP.2006.265.01.05, 2006.

Schäfer, O.: Tektonik und Sedimentation im kontinentalen Saar-Nahe-Becken ("Strike- lip"-Modell, Karbon-Perm,

Westdeutschland), Zeitschrift der Dtsch. Gesellschaft fur Geowissenschaften, 162(2), 127–155, doi:10.1127/1860-

1804/2011/0162-0127, 2011.

665   Schubert, W., Lippolt, H. J. and Schwarz, W.: Early to Middle Carboniferous hornblende 40Ar/39Ar ages of amphibolites

and gabbros from the Bergsträsser Odenwald, Mineral. Petrol., 72(1–3), 113–132, doi:10.1007/s007100170029, 2001.

Schulmann, K., Catalán, J. R. M., Lardeaux, J. M., Janoušek, V. and Oggiano, G.: The Variscan orogeny: Extent, timescale

and the formation of the European crust, Geol. Soc. Spec. Publ., 405(1), 1–6, doi:10.1144/SP405.15, 2014.

Schwarz, M. and Henk, A.: Evolution and structure of the Upper Rhine Graben: Insights from three-dimensional

670   thermomechanical modelling, Int. J. Earth Sci., 94(4), 732–750, doi:10.1007/s00531-004-0451-2, 2005.

von Seckendorff, V., Arz, C. and Lorenz, V.: Magmatism of the late Variscan intermontane Saar-Nahe Basin (Germany): A

review, Geol. Soc. Spec. Publ., 223, 361–391, doi:10.1144/GSL.SP.2004.223.01.16, 2004a.

von Seckendorff, V., Timmerman, M. J., Kramer, W. and Wrobel, P.: New 40Ar/39Ar ages and geochemistry of late

Carboniferous-early Permian lamprophyres and related volcanic rocks in the Saxothuringian Zone of the Variscan Orogen

675   (Germany), Geol. Soc. Spec. Publ., 223, 335–359, doi:10.1144/GSL.SP.2004.223.01.15, 2004b.

Singer, A.: Illite in aridic soils, desert dusts and desert loess, Sediment. Geol., 59(3–4), 251–259, doi:10.1016/0037-

0738(88)90079-6, 1988.

Sissingh, W.: Tertiary paleogeographic and tectonostratigraphic evolution of the Rhenish Triple Junction, Palaeogeogr.

Palaeoclimatol. Palaeoecol., 196(1–2), 229–263, doi:10.1016/S0031-0182(03)00320-1, 2003.

680   Staude, S., Göb, S., Pfaff, K., Ströbele, F., Premo, W. R. and Markl, G.: Deciphering fluid sources of hydrothermal systems:

A combined Sr- and S-isotope study on barite (Schwarzwald, SW Germany), Chem. Geol., 286(1–2), 1–20,

doi:10.1016/j.chemgeo.2011.04.009, 2011.

Stimac, J., Goff, F. and Goff, C. J.: Intrusion-Related Geothermal Systems, Second Edi., Dr Jim Stimac, Copyright © 2015.,

2015.

685   Stipp, M., Stünitz, H., Heilbronner, R. and Schmid, S. M.: Dynamic recrystallization of quartz: Correlation between natural

and experimental conditions, Geol. Soc. Spec. Publ., 200(May 2014), 171–190, doi:10.1144/GSL.SP.2001.200.01.11, 2002.

Stollhofen, H.: Facies architecture variations and seismogenic structures in the Carboniferous-Permian Saar-Nahe Basin (SW

Germany): evidence for extension-related transfer fault activity., 1998.

Timar-Geng, Z., Fügenschuh, B., Schaltegger, U. and Wetzel, A.: The impact of the Jurassic hydrothermal activity on zircon

690   fission track data from the southern Upper Rhine Graben area, Schweizerische Mineral. und Petrogr. Mitteilungen, 84(3),

257–269, 2004.

Timar-Geng, Z., Fügenschuh, B., Wetzel, A. and Dresmann, H.: Low-temperature thermochronology of the flanks of the southern Upper Rhine Graben, Int. J. Earth Sci., 95(4), 685–702, doi:10.1007/s00531-005-0059-1, 2006.

Varajao, A. F. D. C., Gilkes, R. J. and Hart, R. D.: The relationships between kaolinite crystal properties and the origin of

695 materials for a Brazilian kaolin deposit, Clays Clay Miner., 49(1), 44–59, doi:10.1346/CCMN.2001.0490104, 2001.

Vázquez, M., Ramírez, S., Morata, D., Reich, M., Braun, J. J. and Carretier, S.: Regolith production and chemical weathering of granitic rocks in central Chile, Chem. Geol., 446, 87–98, doi:10.1016/j.chemgeo.2016.09.023, 2016.

Wagner, G. A., Kernphysik, M. and Heidelberg, D.-: Crystalline Basement of Middle Europe, Tracks A J. Artist. Writings, 17(3), 277–282, 1990.

700 Willner, A. P., Massonne, H. J. and Krohe, A.: Tectono-thermal evolution of a part of a Variscan magmatic arc: The Odenwald in the Mid-German Crystalline Rise, Geol. Rundschau, 80(2), 369–389, doi:10.1007/BF01829372, 1991.

Zeh, A. and Brätz, H.: Timing of Upper Carboniferous-Permian horst-basin formation and magmatism in the NW Thuringian Forest, central Germany: A review, Geol. Soc. Spec. Publ., 223, 319–334, doi:10.1144/GSL.SP.2004.223.01.14, 2004.

Zeh, A. and Gerdes, A.: Baltica- and Gondwana-derived sediments in the Mid-German Crystalline Rise (Central Europe):

705 Implications for the closure of the Rheic ocean, Gondwana Res., 17(2–3), 254–263, doi:10.1016/j.gr.2009.08.004, 2010.

Zeh, A. and Will, T. M.: The mid-German crystalline zone, Pre-Mesozoic Geol. Saxo-Thuringia. From Cadomian Act. Margin to Variscan Orogen, 195–220, 2008.

Zhou, L., Friis, H., Yang, T. and Nielsen, A. T.: Geochemical interpretation of the Precambrian basement and overlying Cambrian sandstone on Bornholm, Denmark: Implications for the weathering history, Lithos, 286–287, 369–387,

710 doi:10.1016/j.lithos.2017.06.019, 2017.

Ziegler, P. A., Schumacher, M. E., Dèzes, P., van Wees, J. D. and Cloetingh, S.: Post-Variscan evolution of the lithosphere in the Rhine Graben area: Constraints from subsidence modelling, Geol. Soc. Spec. Publ., 223, 289–317, doi:10.1144/GSL.SP.2004.223.01.13, 2004.